US 20180360320A1

(19) United States

(12) Patent Application Publication (10) Pub. No.: US 2018/0360320 A1

Werahera et al. (43) Pub. Date: Dec. 20, 2018

(54) MULTI-EXCITATION DIAGNOSTIC SYSTEM AND METHODS FOR CLASSIFICATION OF TISSUE

(71) Applicant: **The Regents of the University of Colorado, a body corporate**, Denver, CO (US)

(72) Inventors: **Priya N. Werahera**, Aurora, CA (US); **John Daily**, Lafayette, CO (US); **M. Scott Lucia**, Larkspur, CO (US); **Adrie van Bokhoven**, Denver, CO (US); **E. David Crawford**, Denver, CO (US); **Frank Barnes**, Boulder, CO (US)

(21) Appl. No.: **16/036,323**

(22) Filed: **Jul. 16, 2018**

Related U.S. Application Data

(63) Continuation of application No. 13/691,067, filed on Nov. 30, 2012, now abandoned, which is a continuation of application No. 11/913,042, filed on Oct. 29, 2007, now Pat. No. 8,406,858, filed as application No. PCT/US06/16587 on May 1, 2006.

(60) Provisional application No. 60/676,420, filed on Apr. 29, 2005, provisional application No. 60/718,194, filed on Sep. 15, 2005.

Publication Classification

(51) **Int. Cl.**
A61B 5/00 (2006.01)

(52) **U.S. Cl.**
CPC ***A61B 5/0082*** (2013.01); ***A61B 5/7267*** (2013.01); ***A61B 5/0059*** (2013.01)

(57) **ABSTRACT**

Methods and systems for in vivo classification of tissue are disclosed. The tissue is irradiated with light from multiple light sources and light scattered and fluoresced from the tissue is received. Distinct emissions of the sample are identified from the received light. An excitation-emission matrix is generated (**1002**). On-diagonal and off-diagonal components of the excitation-emission matrix are identified (**1004**, **1006**, **1008**). Spectroscopic measures are derived from the excitation-emission matrix (**1014**), and are compared to a database of known spectra (**1016**) permitting the tissue to be classified as benign or malignant (**1018**). An optical biopsy needle or an optical probe may be used to contemporaneously classify and sample tissue for pathological confirmation of diagnosis.

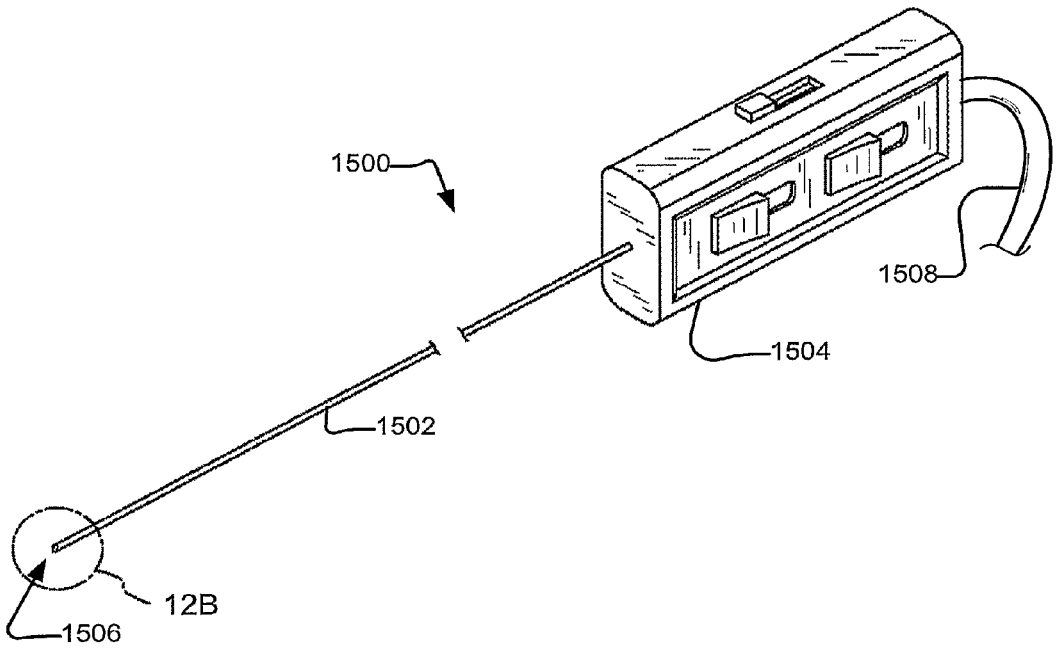

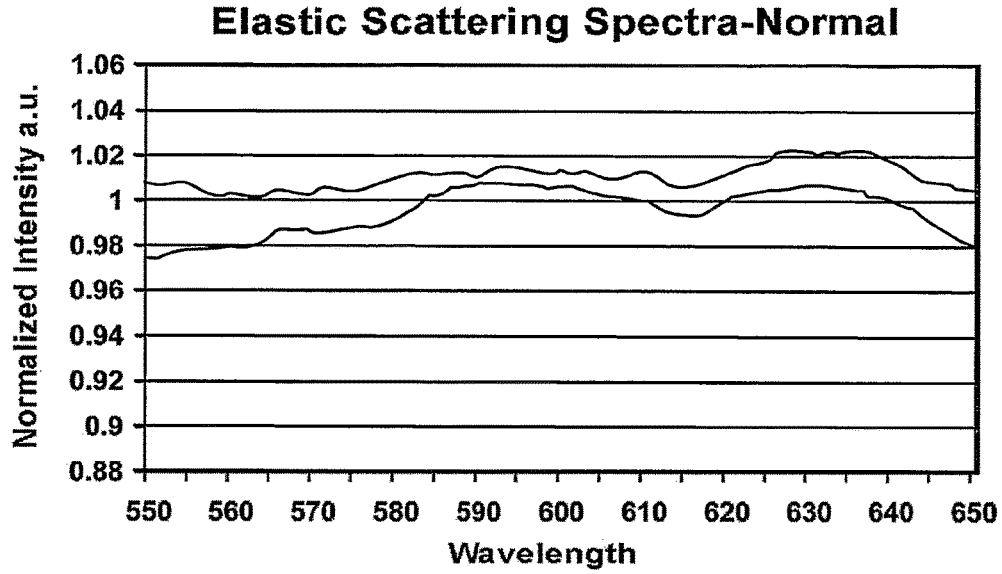
Elastic Scattering Spectra-Normal
Normalized Intensity a.u.
1.06
1.04
1.02
1
0.98
0.96
0.94
0.92
0.9
0.88
550 560 570 580 590 600 610 620 630 640 650
Wavelength

Fig. 1A

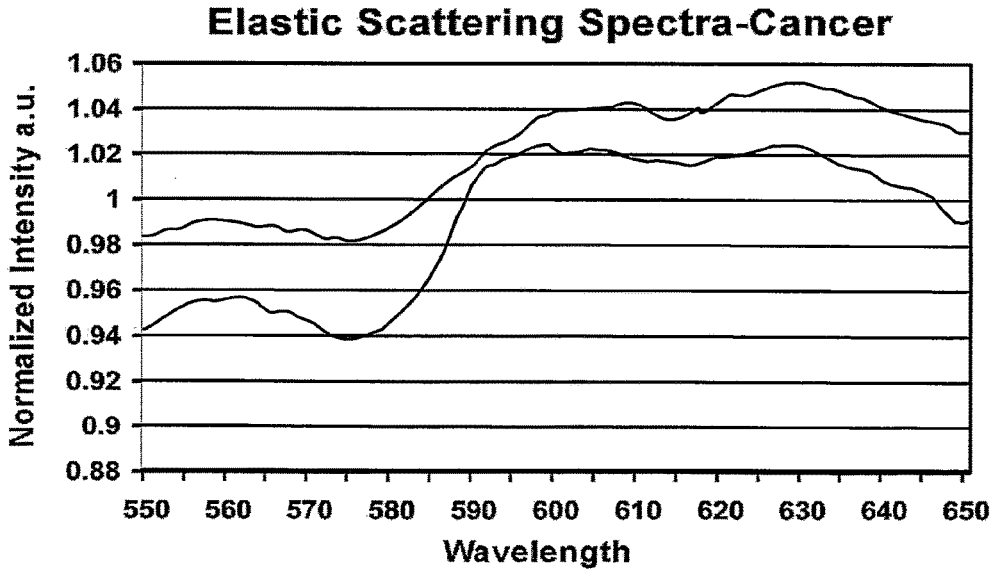
Elastic Scattering Spectra-Cancer
Normalized Intensity a.u.
1.06
1.04
1.02
1
0.98
0.96
0.94
0.92
0.9
0.88
550 560 570 580 590 600 610 620 630 640 650
Wavelength

Fig. 1B

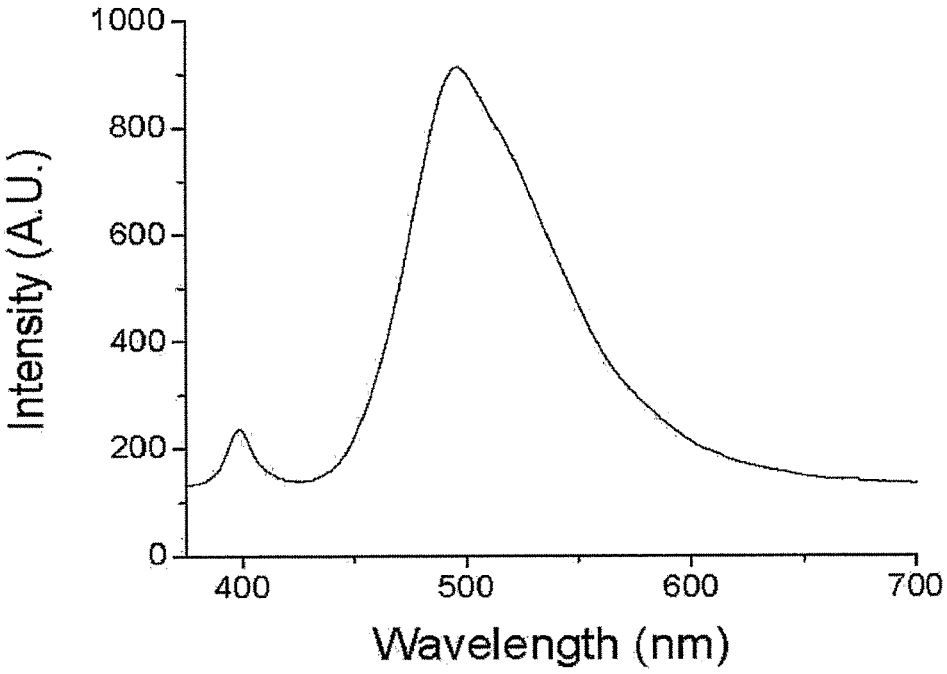
1000
800
600
400
200
0
Intensity (A.U.)
400
500
600
700
Wavelength (nm)

Fig. 2

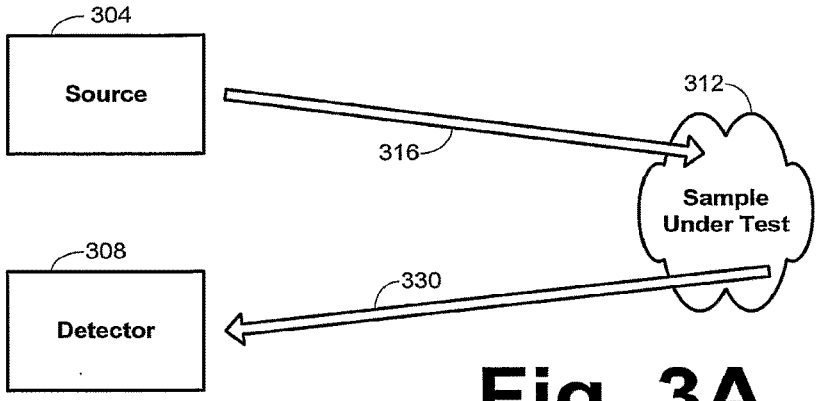

Fig. 3A

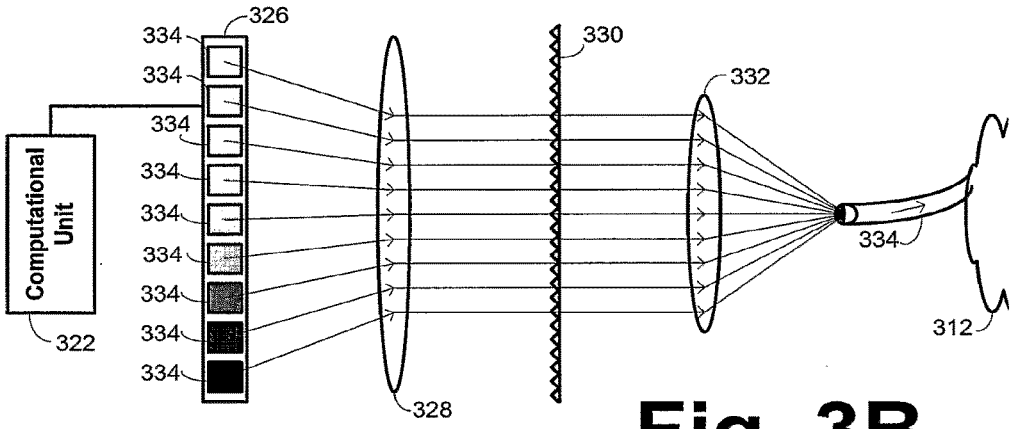

Fig. 3B

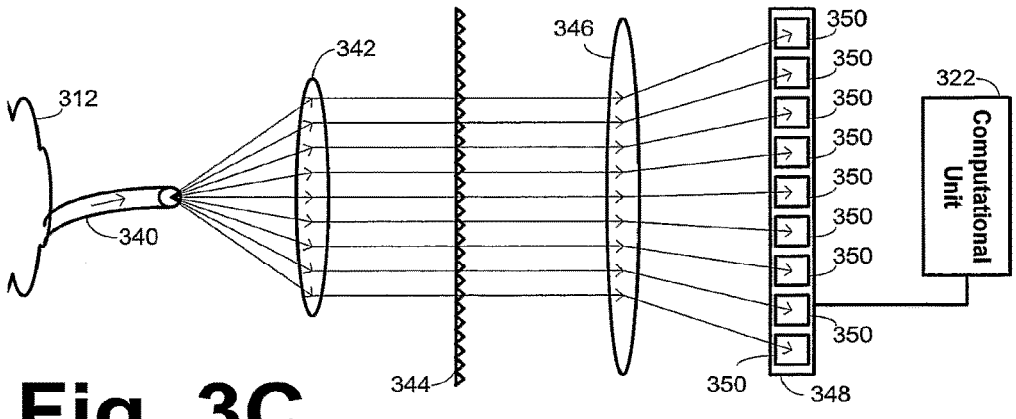

Fig. 3C

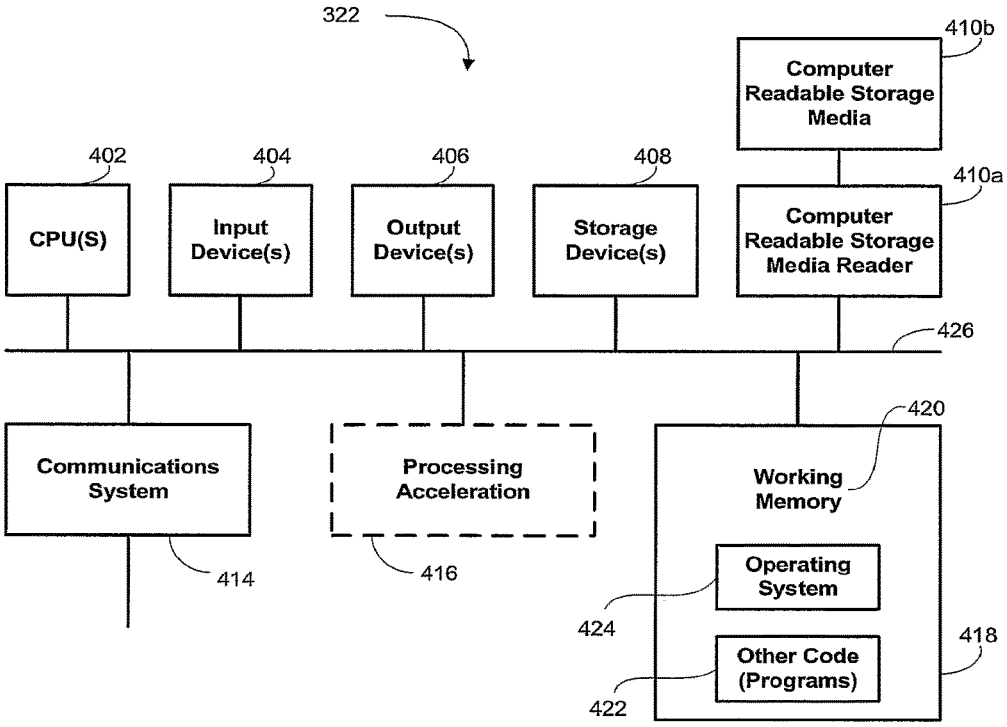
322
410b
Computer Readable Storage Media
402
404
406
408
410a
CPU(S)
Input Device(s)
Output Device(s)
Storage Device(s)
Computer Readable Storage Media Reader
426
420
Communications System
Processing Acceleration
Working Memory
Operating System
424
Other Code (Programs)
418
422
414
416

Fig. 4

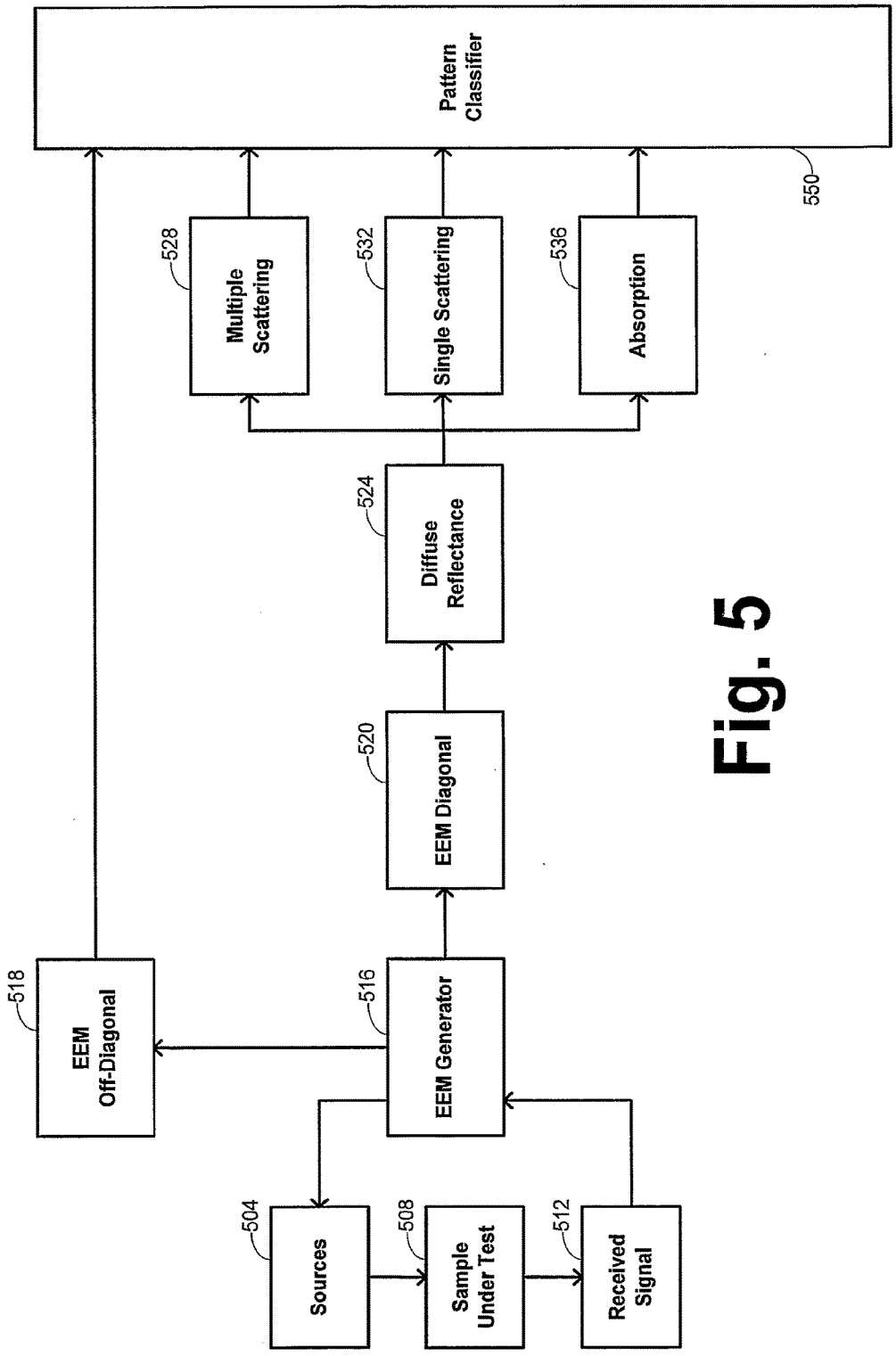
Pattern Classifier
550
528
Multiple Scattering
532
Single Scattering
536
Absorption
524
Diffuse Reflectance
520
EEM Diagonal
516
EEM Generator
518
EEM Off-Diagonal
504
Sources
508
Sample Under Test
512
Received Signal

Fig. 5

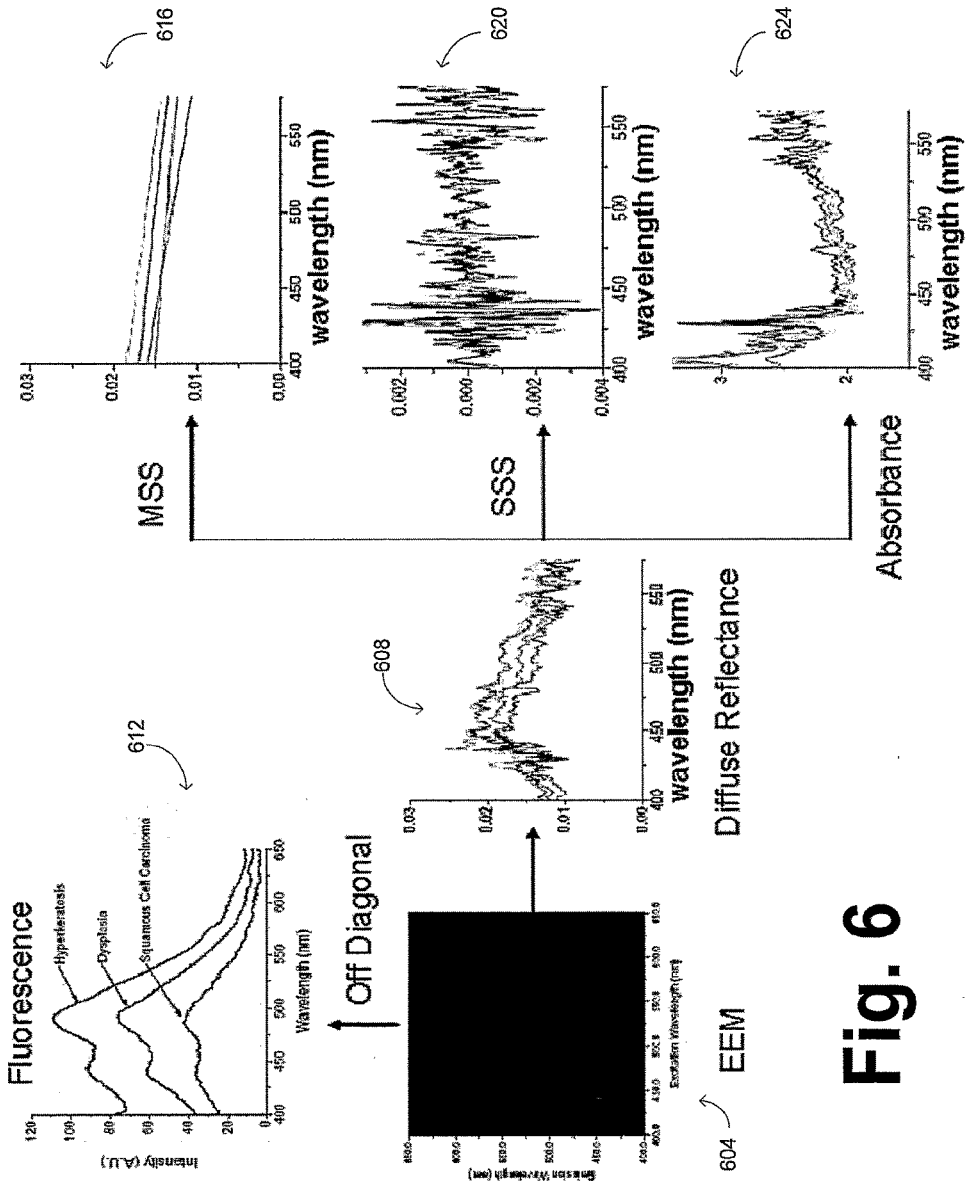
Fluorescence
Hyperkeratosis
Dysplasia
Squamous Cell Carcinoma
Intensity (A.U.)
Wavelength (nm)
612
Off Diagonal
608
wavelength (nm)
EEM
604
Diffuse Reflectance
MSS
SSS
Absorbance
616
620
624
wavelength (nm)
wavelength (nm)
wavelength (nm)

Fig. 6

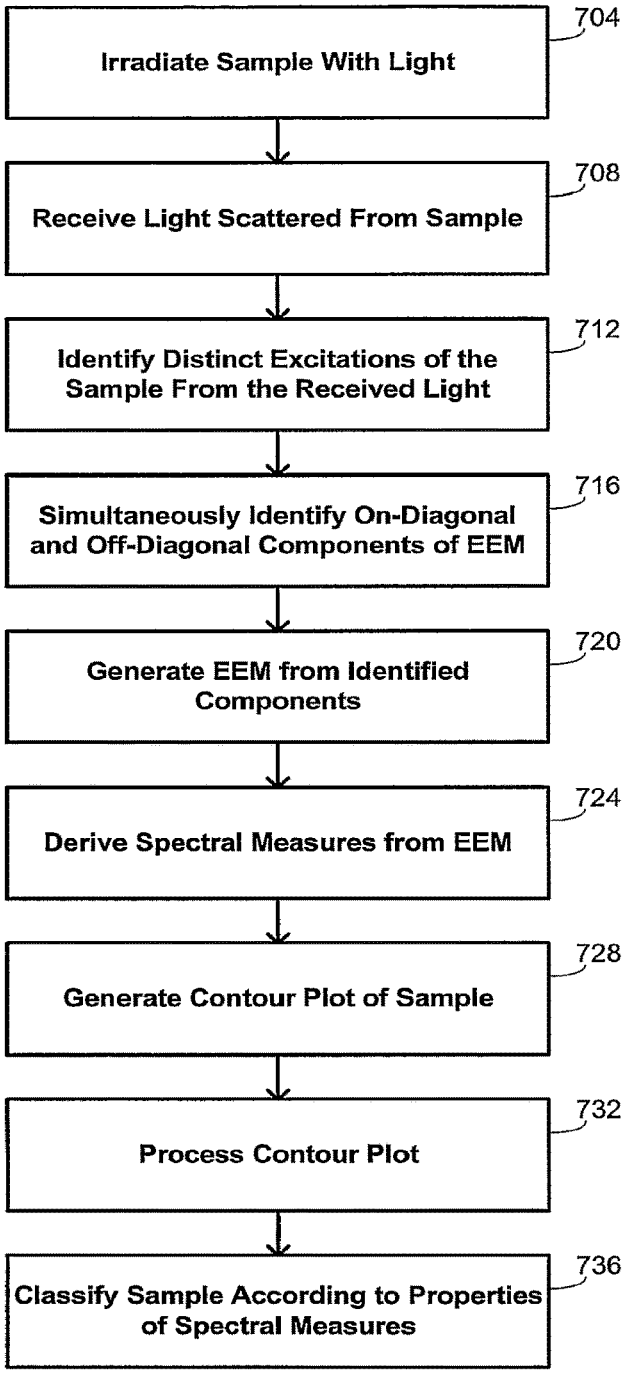
Irradiate Sample With Light
704
Receive Light Scattered From Sample
708
Identify Distinct Excitations of the Sample From the Received Light
712
Simultaneously Identify On-Diagonal and Off-Diagonal Components of EEM
716
Generate EEM from Identified Components
720
Derive Spectral Measures from EEM
724
Generate Contour Plot of Sample
728
Process Contour Plot
732
Classify Sample According to Properties of Spectral Measures
736

Fig. 7

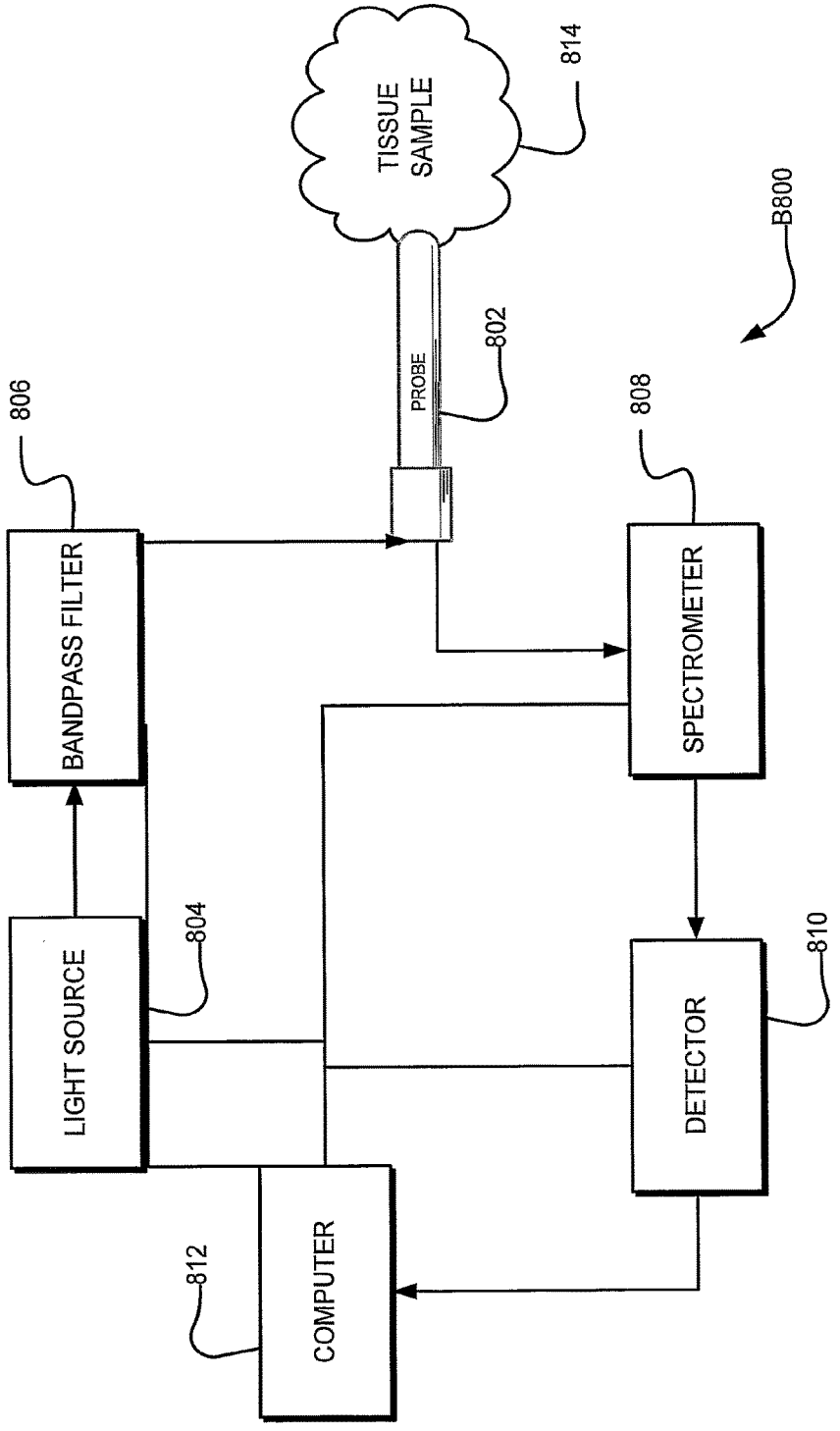
TISSUE SAMPLE
814
B800
PROBE
802
806
808
BANDPASS FILTER
SPECTROMETER
LIGHT SOURCE
804
DETECTOR
810
COMPUTER
812

Fig. 8

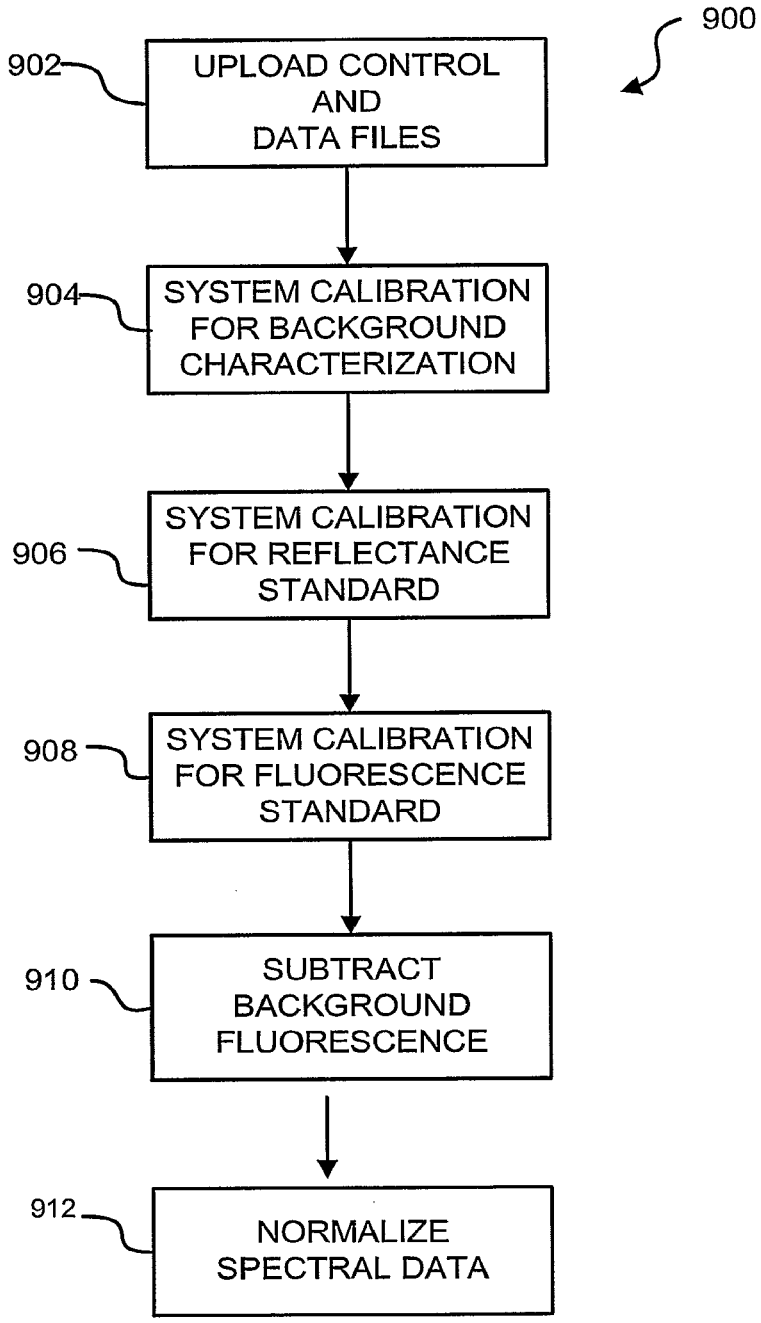
900
902
UPLOAD CONTROL AND DATA FILES
904
SYSTEM CALIBRATION FOR BACKGROUND CHARACTERIZATION
906
SYSTEM CALIBRATION FOR REFLECTANCE STANDARD
908
SYSTEM CALIBRATION FOR FLUORESCENCE STANDARD
910
SUBTRACT BACKGROUND FLUORESCENCE
912
NORMALIZE SPECTRAL DATA

Fig. 9

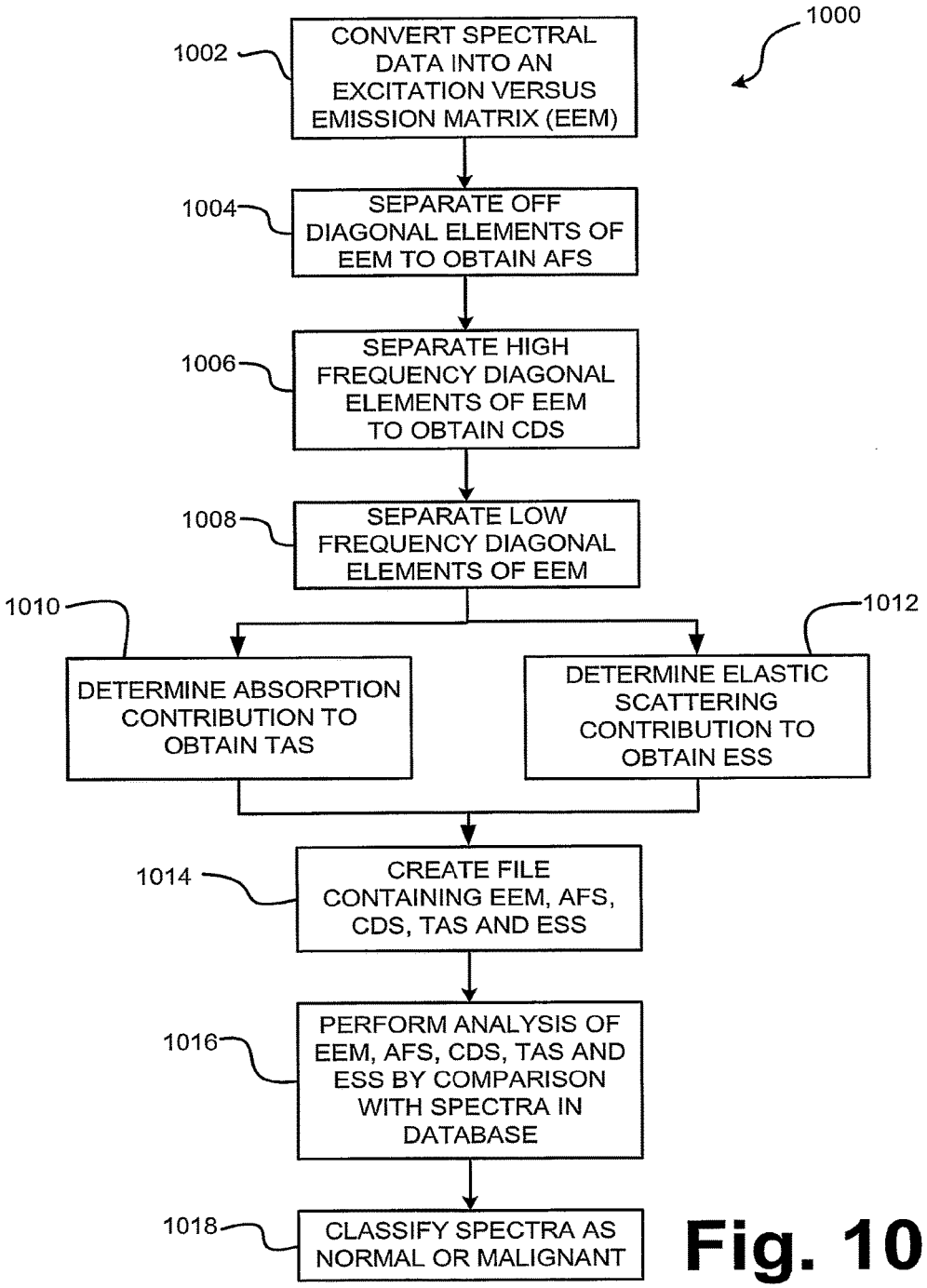
1000
1002
CONVERT SPECTRAL DATA INTO AN EXCITATION VERSUS EMISSION MATRIX (EEM)
1004
SEPARATE OFF DIAGONAL ELEMENTS OF EEM TO OBTAIN AFS
1006
SEPARATE HIGH FREQUENCY DIAGONAL ELEMENTS OF EEM TO OBTAIN CDS
1008
SEPARATE LOW FREQUENCY DIAGONAL ELEMENTS OF EEM
1010
DETERMINE ABSORPTION CONTRIBUTION TO OBTAIN TAS
1012
DETERMINE ELASTIC SCATTERING CONTRIBUTION TO OBTAIN ESS
1014
CREATE FILE CONTAINING EEM, AFS, CDS, TAS AND ESS
1016
PERFORM ANALYSIS OF EEM, AFS, CDS, TAS AND ESS BY COMPARISON WITH SPECTRA IN DATABASE
1018
CLASSIFY SPECTRA AS NORMAL OR MALIGNANT

Fig. 10

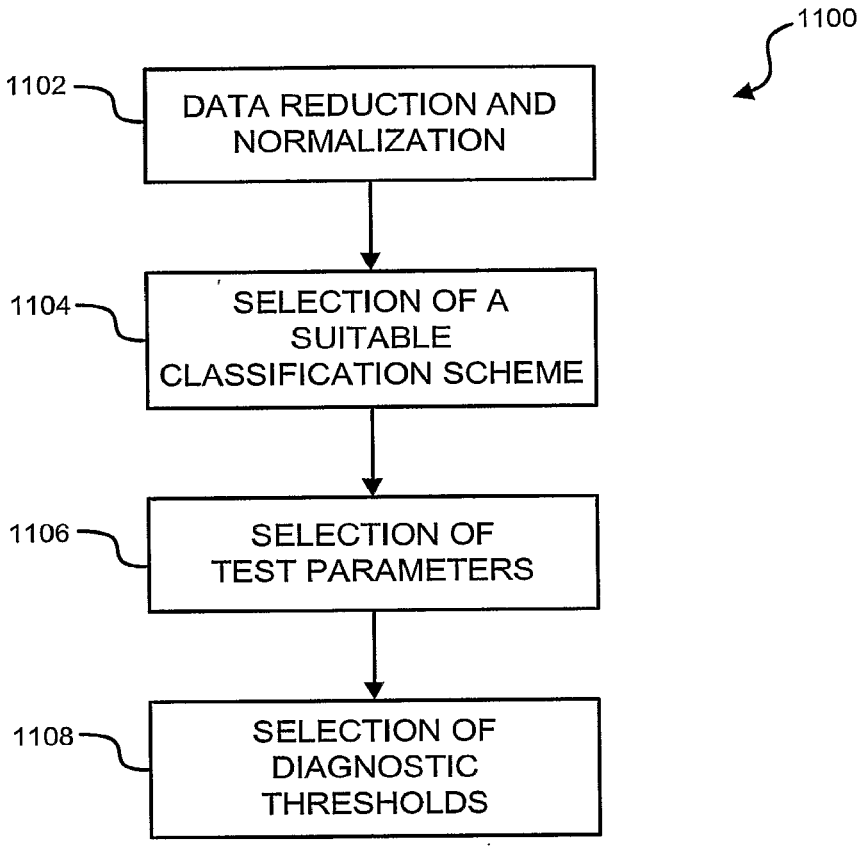
1100
1102
DATA REDUCTION AND NORMALIZATION
1104
SELECTION OF A SUITABLE CLASSIFICATION SCHEME
1106
SELECTION OF TEST PARAMETERS
1108
SELECTION OF DIAGNOSTIC THRESHOLDS

Fig. 11

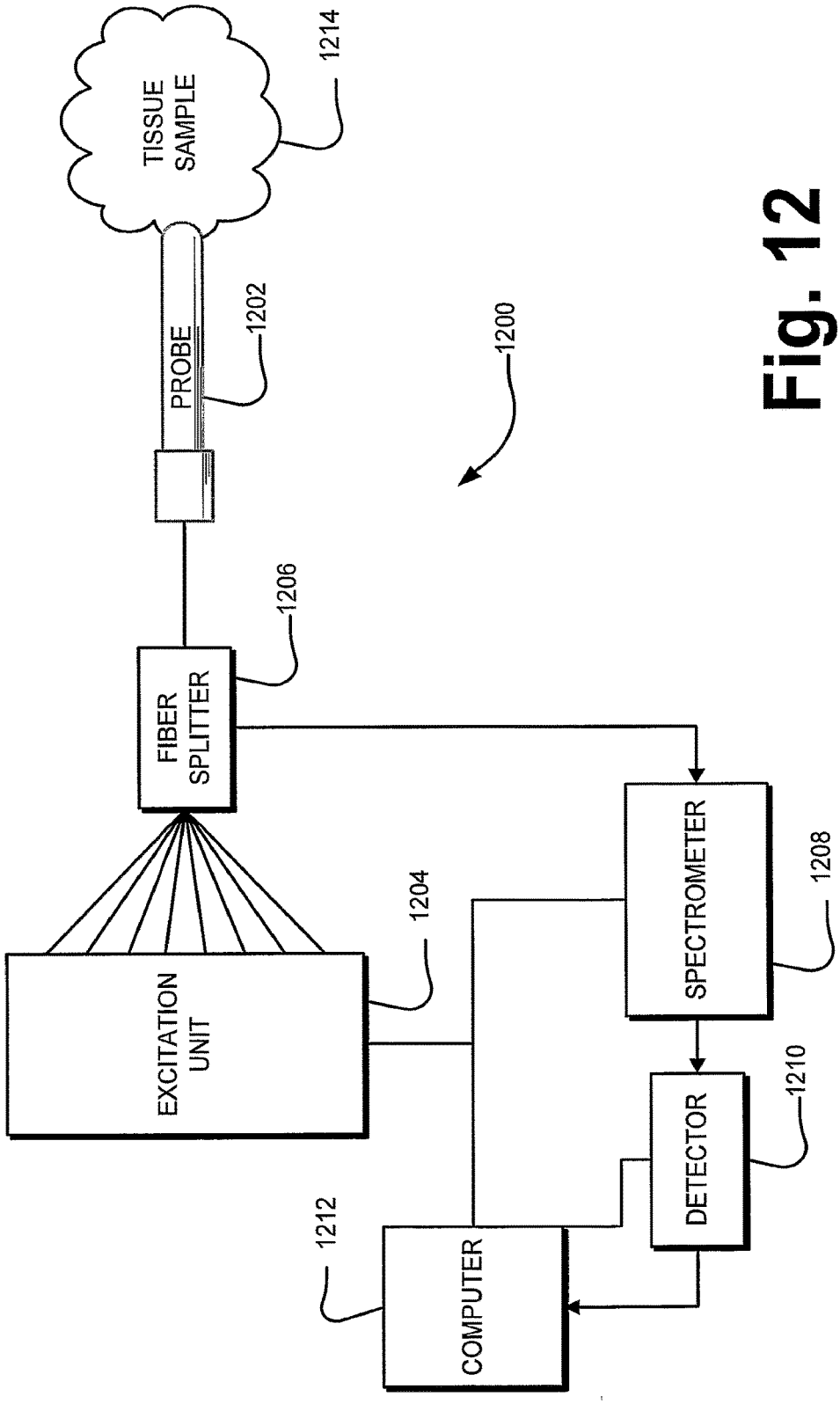
TISSUE SAMPLE
1214
PROBE
1202
1200
FIBER SPLITTER
1206
EXCITATION UNIT
1204
SPECTROMETER
1208
DETECTOR
1210
COMPUTER
1212

Fig. 12

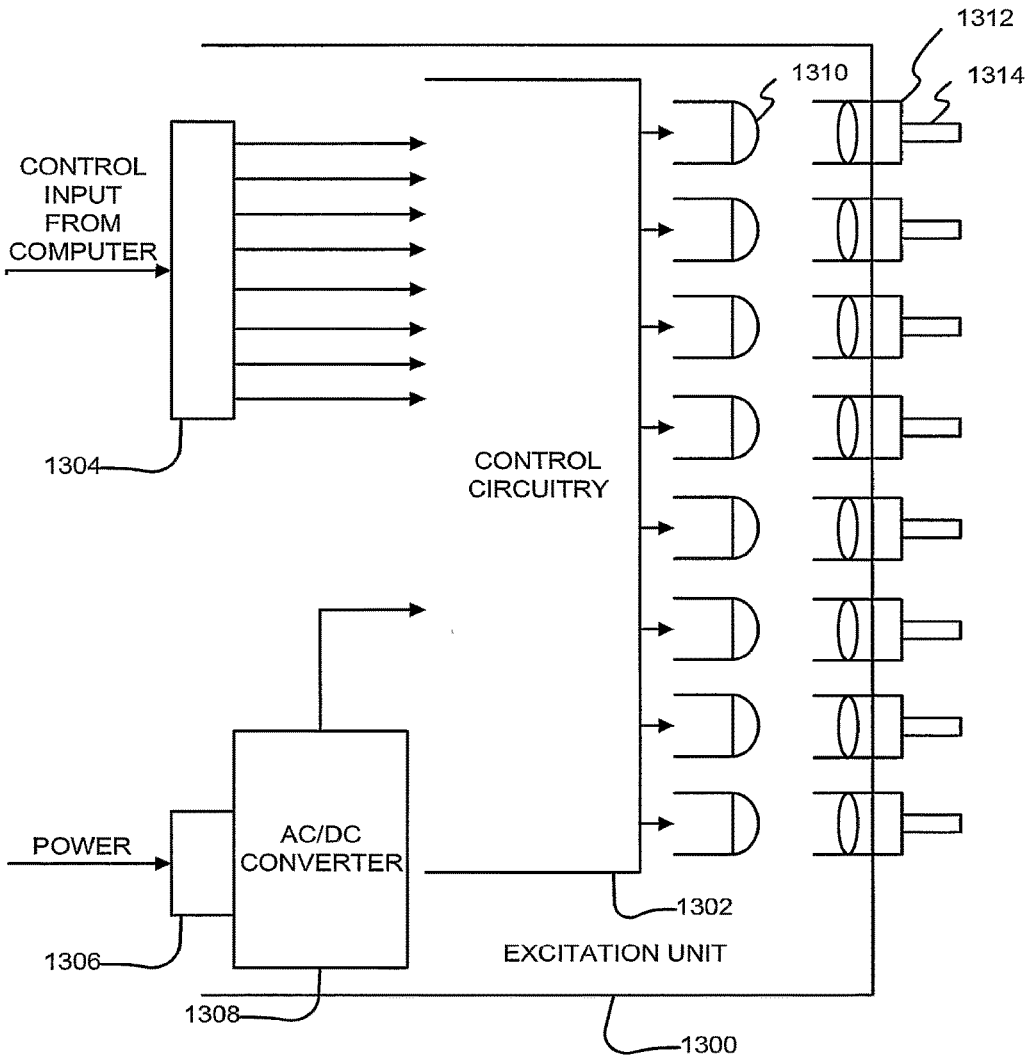
1312
1310
1314
CONTROL INPUT FROM COMPUTER
1304
CONTROL CIRCUITRY
POWER
AC/DC CONVERTER
1306
1308
1302
EXCITATION UNIT
1300

Fig. 13

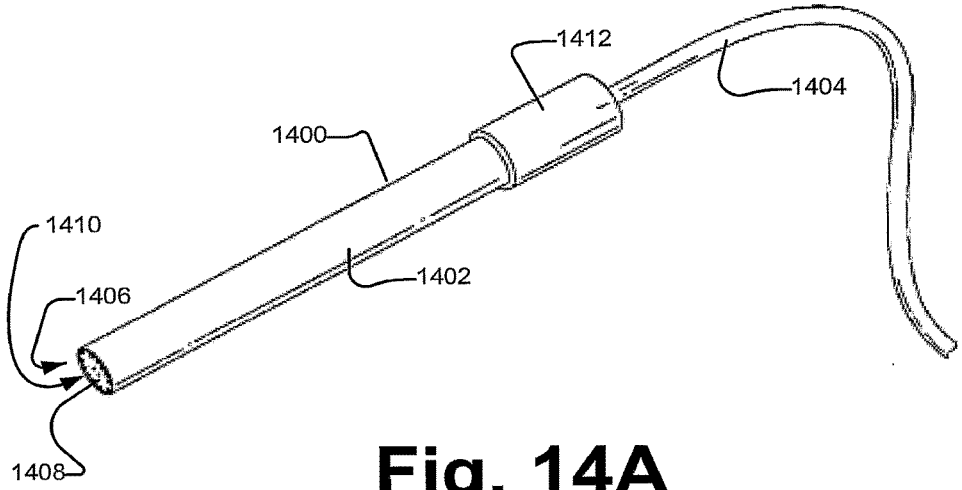

Fig. 14A

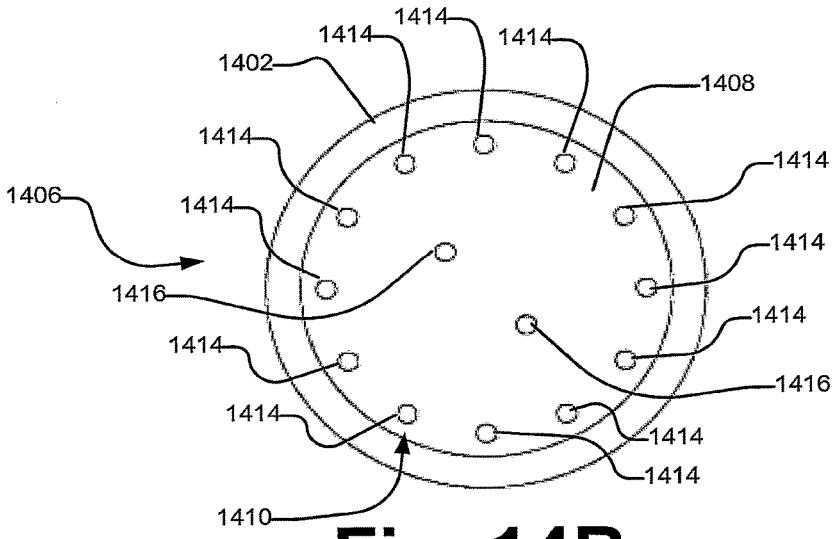

Fig. 14B

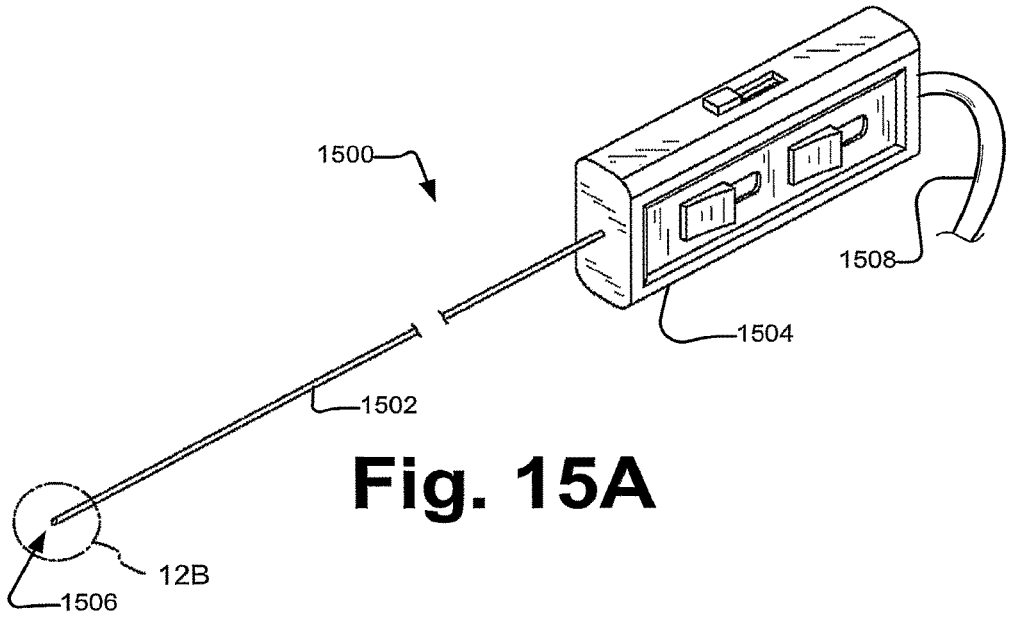

Fig. 15A

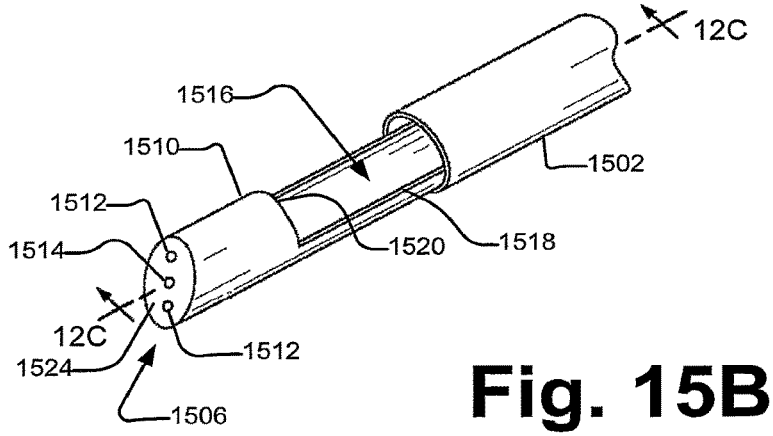

Fig. 15B

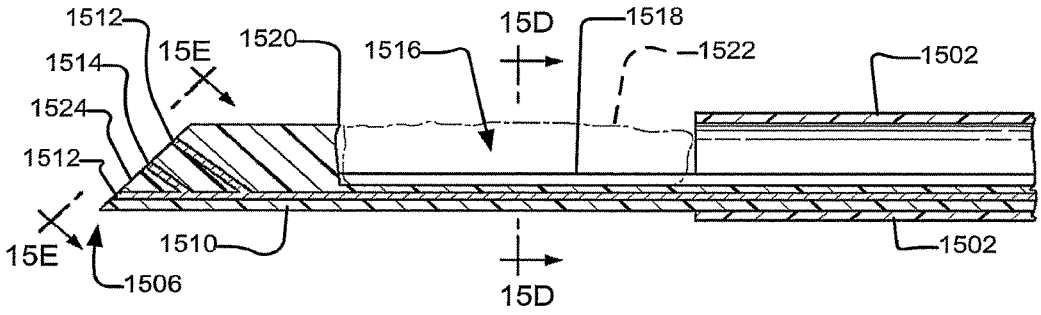

Fig. 15C

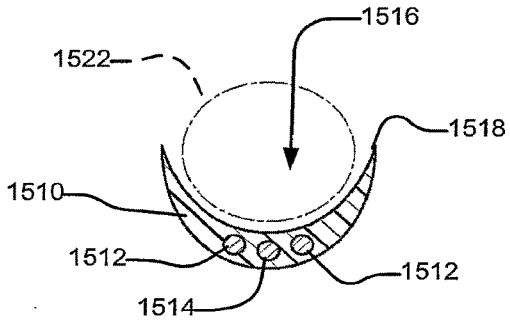

Fig. 15D

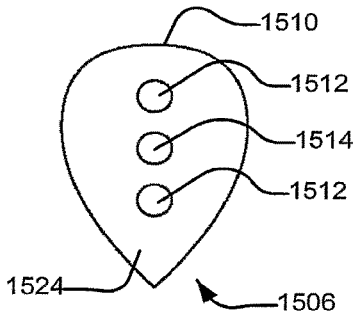

Fig. 15E

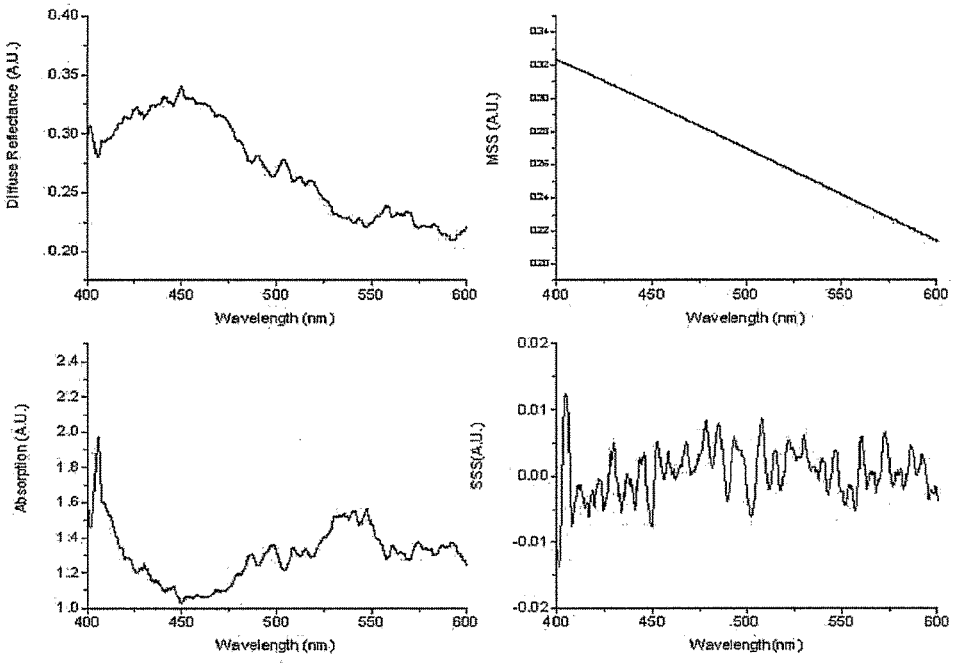
Diffuse Reflectance (A.U.)
0.40
0.35
0.30
0.25
0.20
400
450
500
550
600
Wavelength (nm)
MSS (A.U.)
Wavelength (nm)
Absorption (A.U.)
2.4
2.2
2.0
1.8
1.6
1.4
1.2
1.0
Wavelength (nm)
SSS(A.U.)
0.02
0.01
0.00
-0.01
-0.02
Wavelength(nm)

Fig. 16

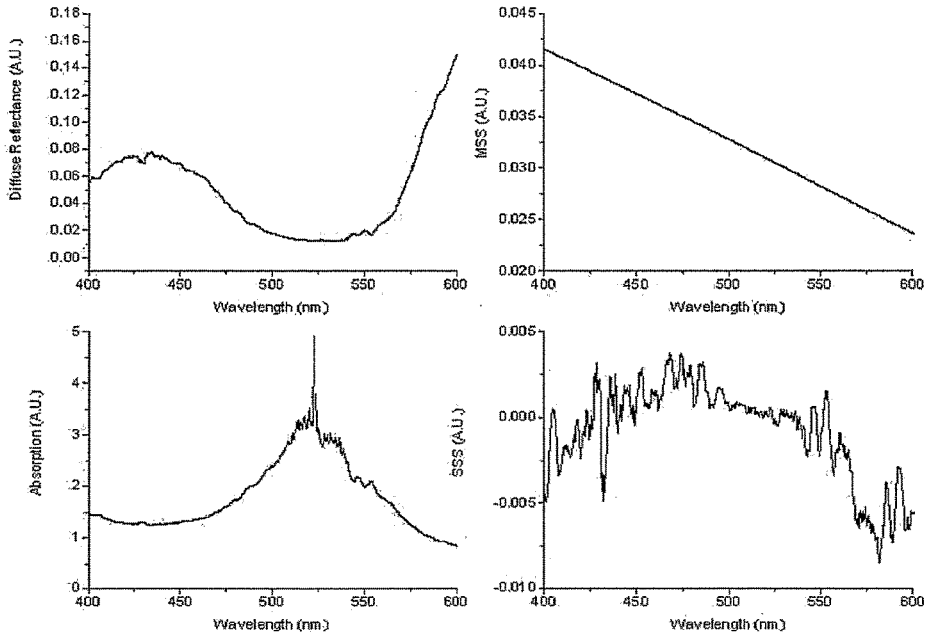
Diffuse Reflectance (A.U.)
Wavelength (nm)
MSS (A.U.)
Wavelength (nm)
Absorption (A.U.)
Wavelength (nm)
SSS (A.U.)
Wavelength (nm)

Fig. 17

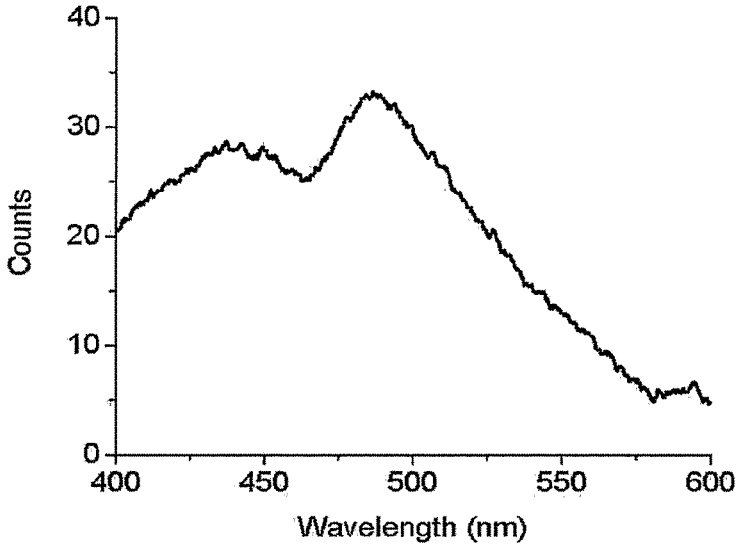

Fig. 18A

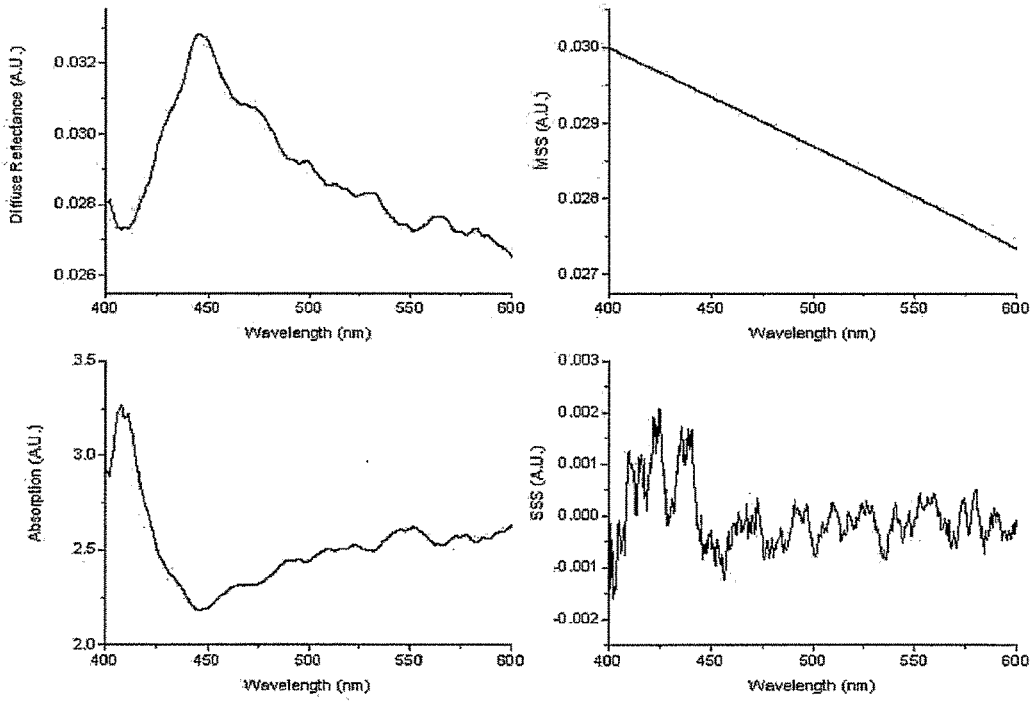

Fig. 18B

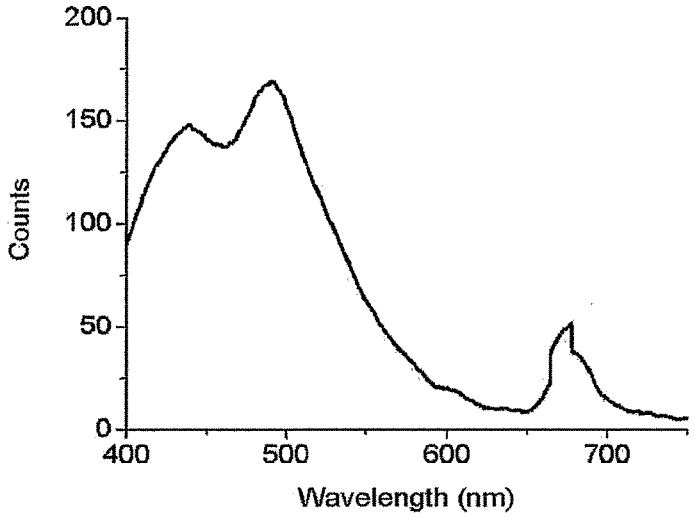

Fig. 19A

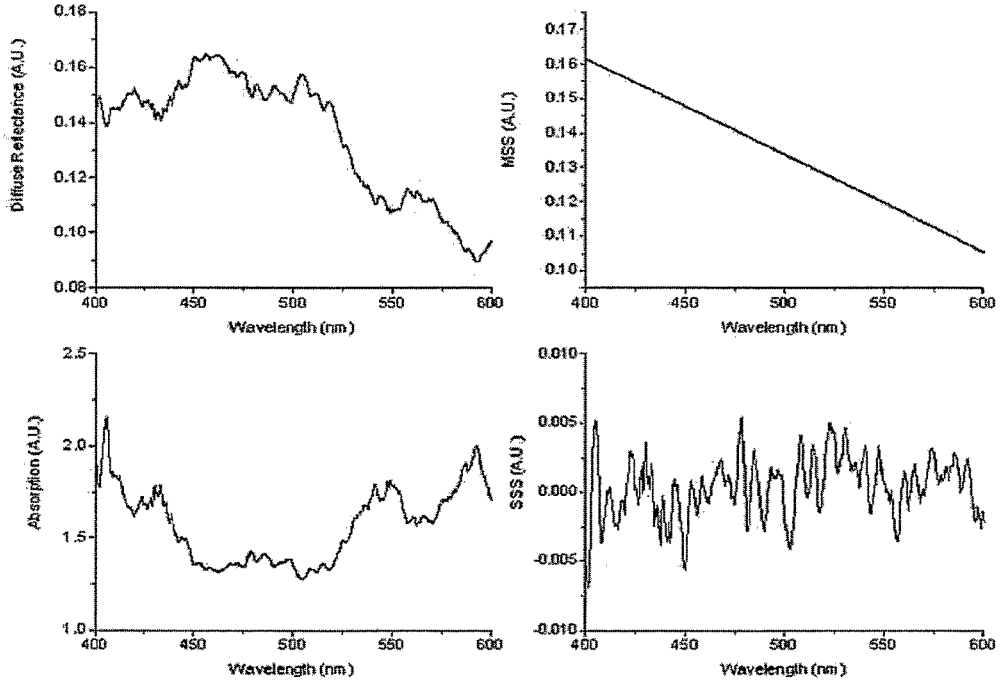

Fig. 19B

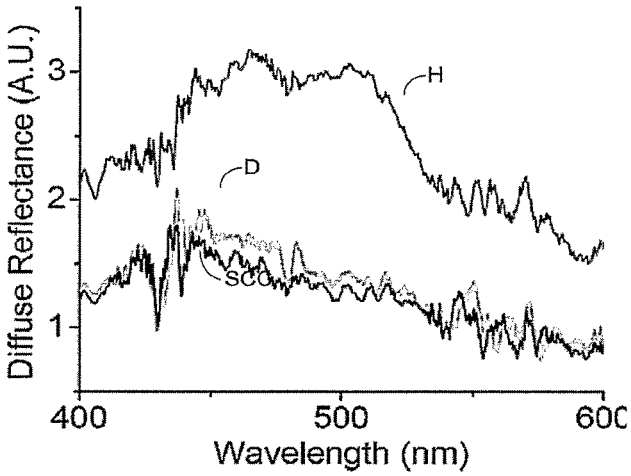
Diffuse Reflectance (A.U.)
3
2
1
H
D
SCC
400
500
600
Wavelength (nm)

Fig. 20

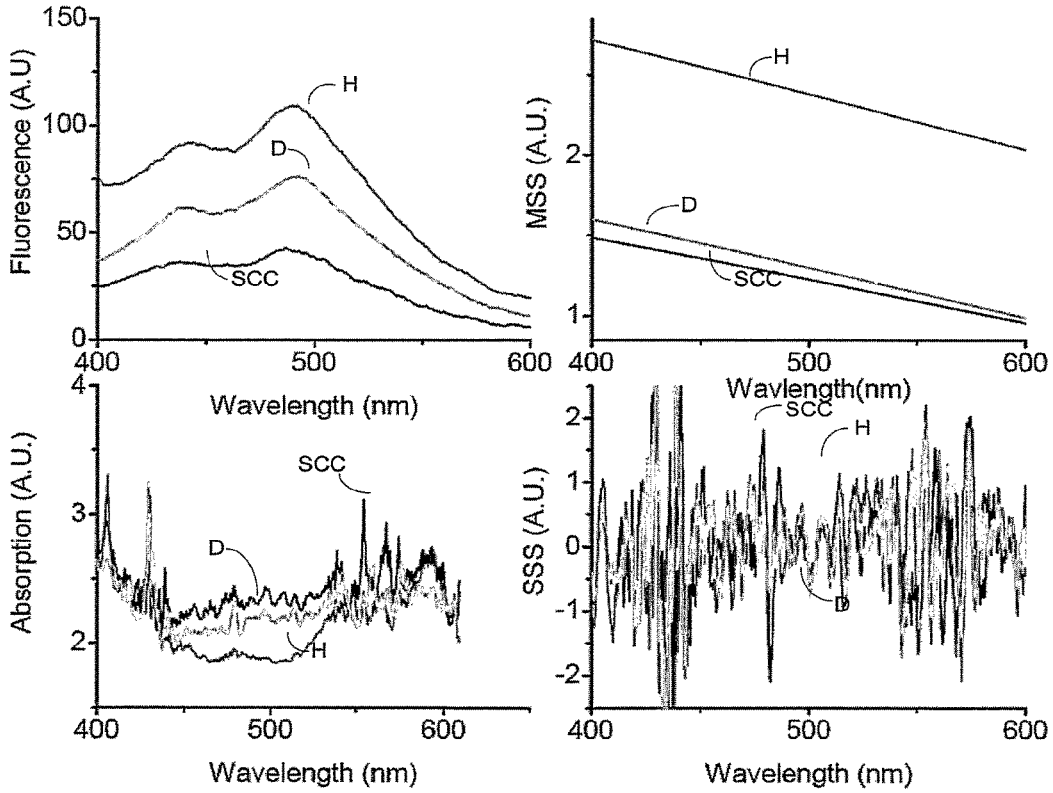
Fluorescence (A.U)
150
100
50
0
H
D
SCC
400
500
600
Wavelength (nm)
MSS (A.U.)
2
1
H
D
SCC
400
500
600
Wavlength(nm)
Absorption (A.U.)
4
3
2
SCC
D
H
400
500
600
Wavelength (nm)
SSS (A.U.)
2
1
0
-1
-2
SCC
H
D
400
500
600
Wavelength (nm)

Fig. 21

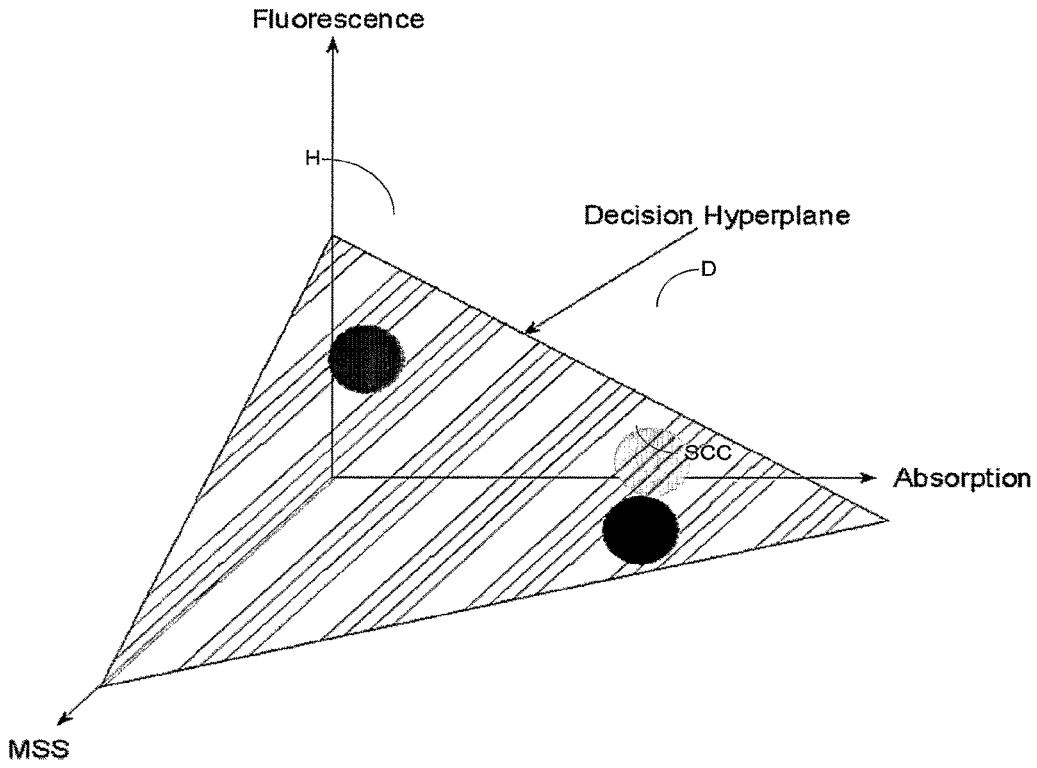

Fig. 22

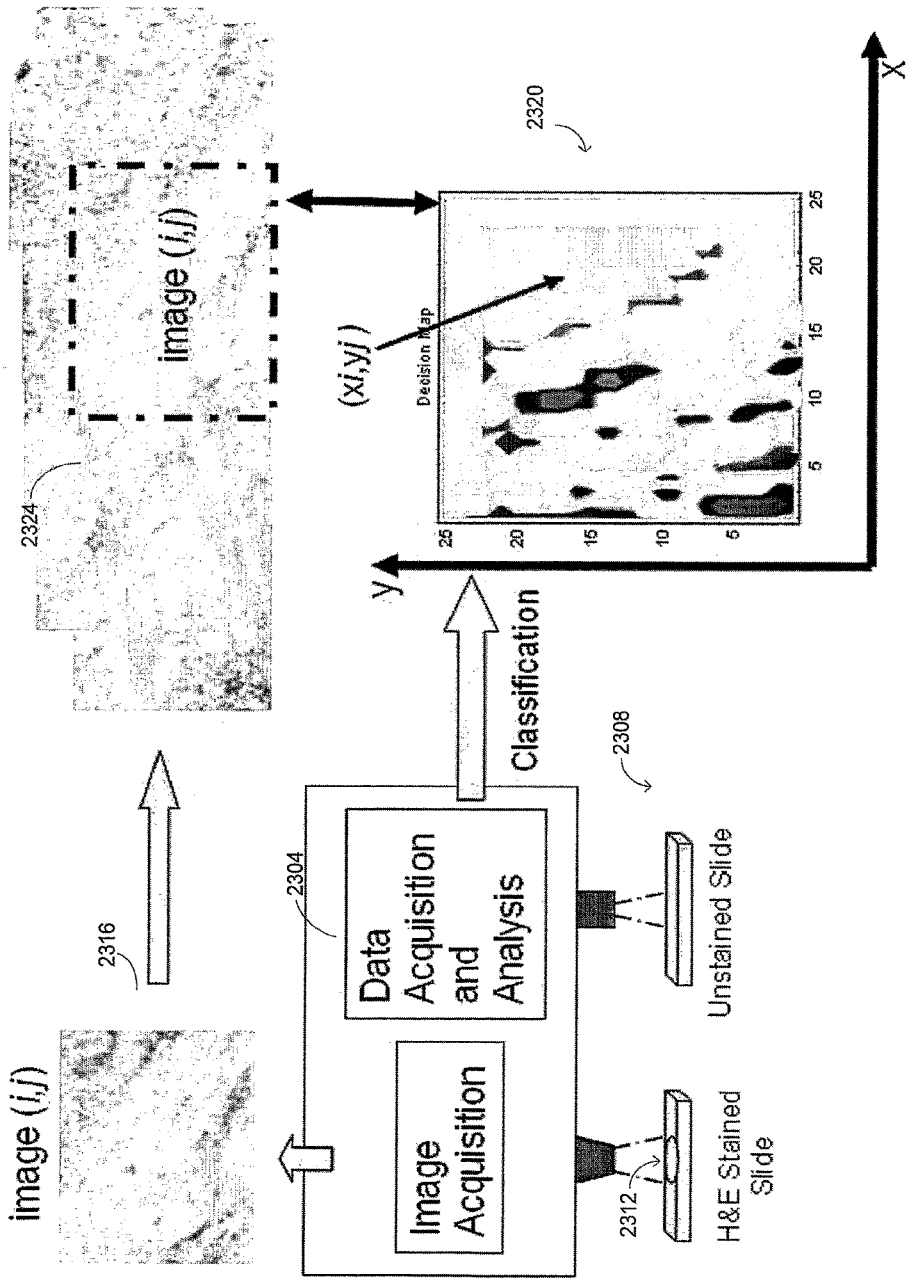
image (i,j)
2316
2304
Data Acquisition and Analysis
Image Acquisition
2312
H&E Stained Slide
2308
Unstained Slide
Classification
2320
Decision Map
(xi,yj)
2324
image (i,j)
y
x

Fig. 23

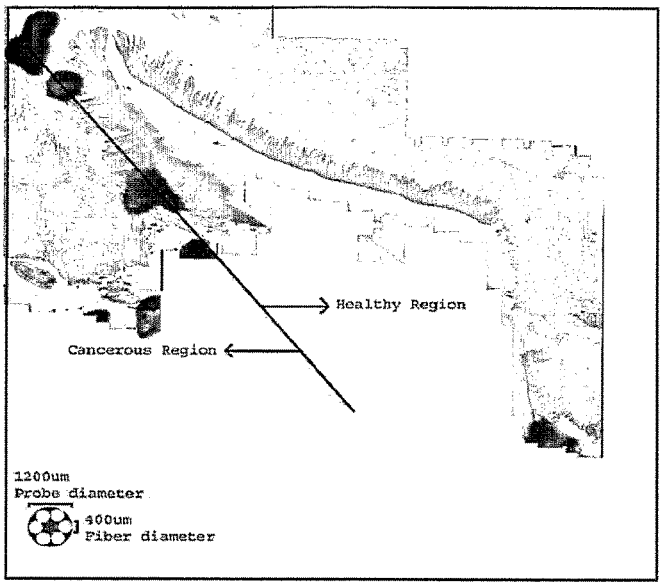

Fig. 24A

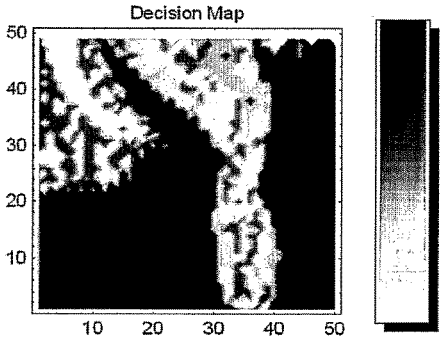

Fig. 24B

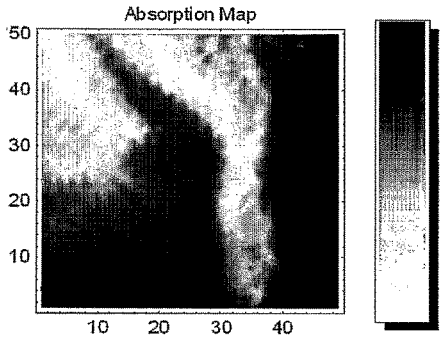

Fig. 24C

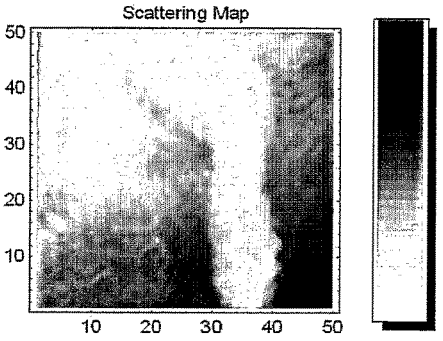

Fig. 24D

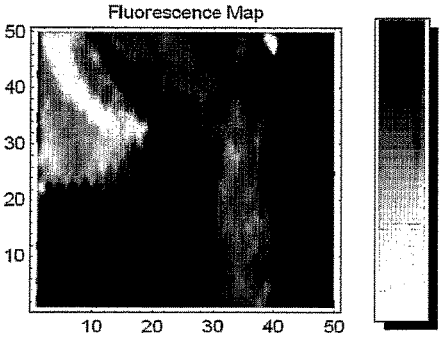

Fig. 24E

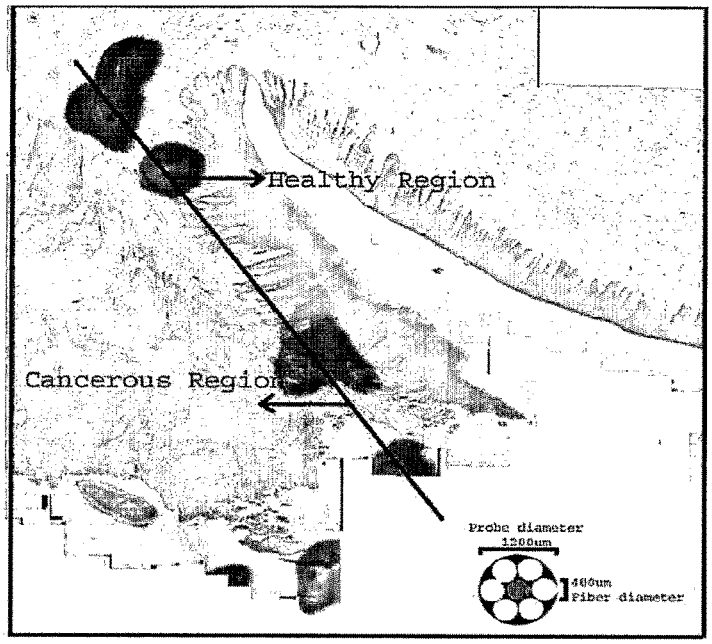

Fig. 25A

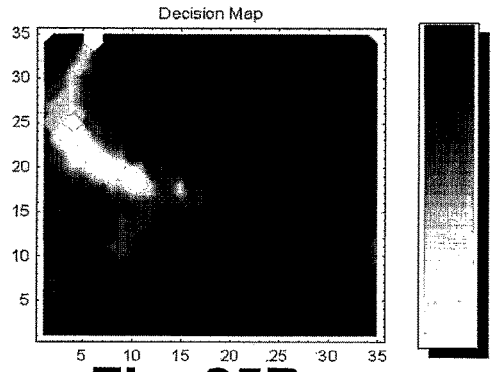

Fig. 25B

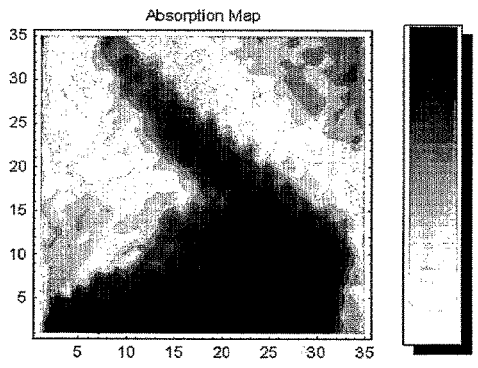

Fig. 25C

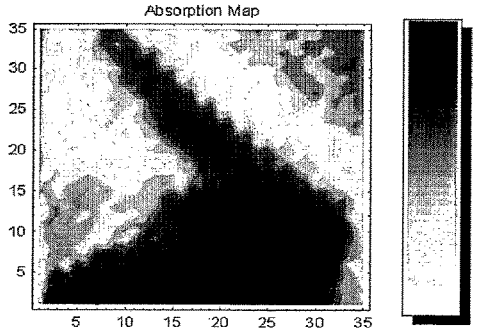

Fig. 25D

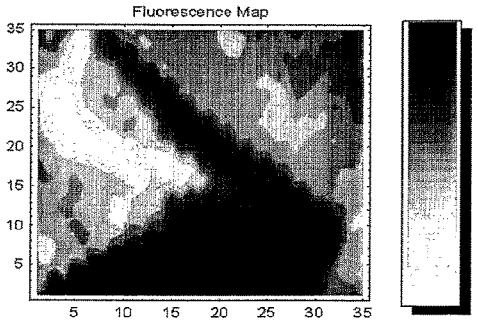

Fig. 25E

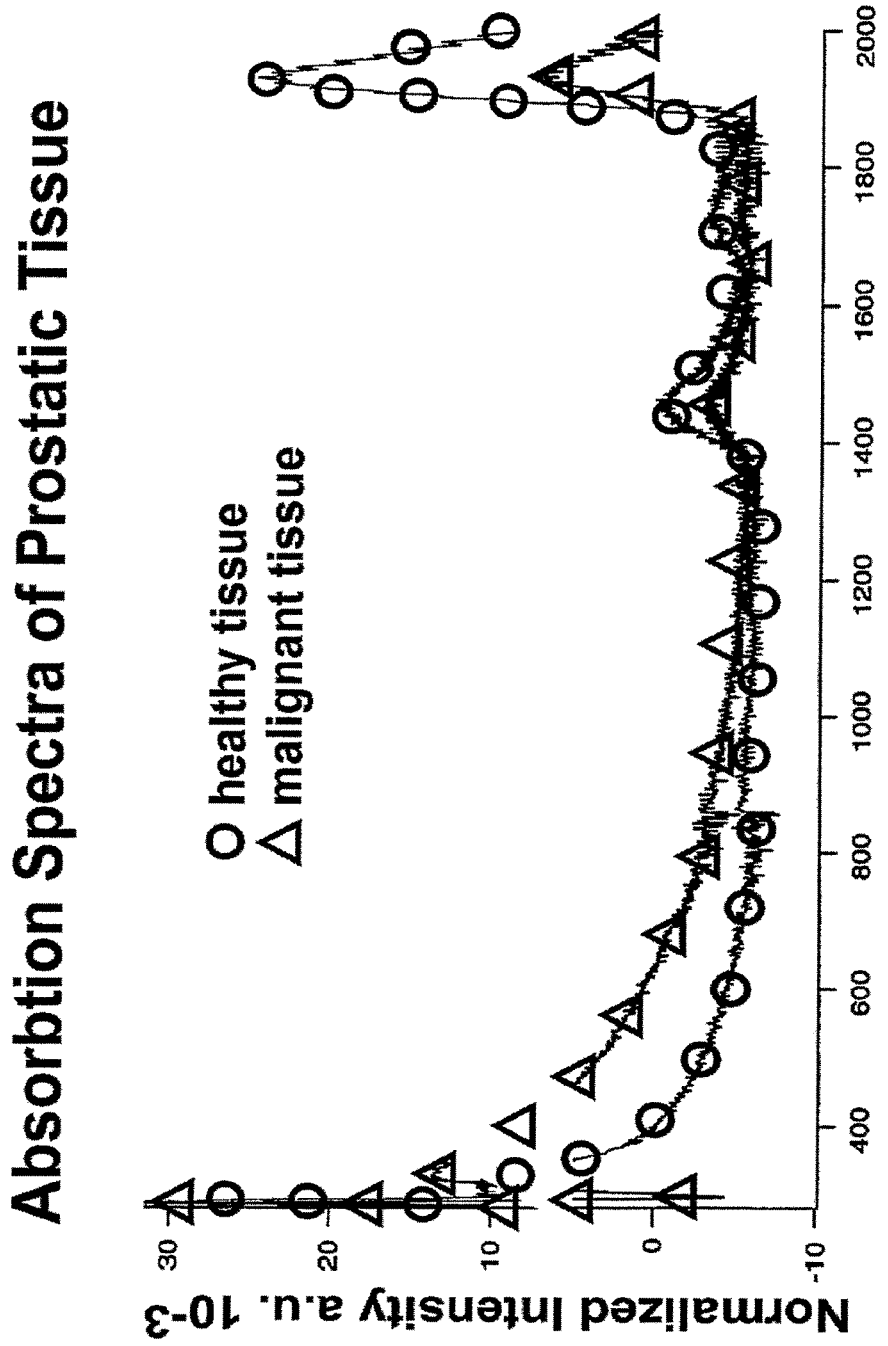
Absorbtion Spectra of Prostatic Tissue
O healthy tissue
Δ malignant tissue
Normalized Intensity a.u. 10-3
30
20
10
0
-10
400
600
800
1000
1200
1400
1600
1800
2000
wavelength (nm)

Fig. 26

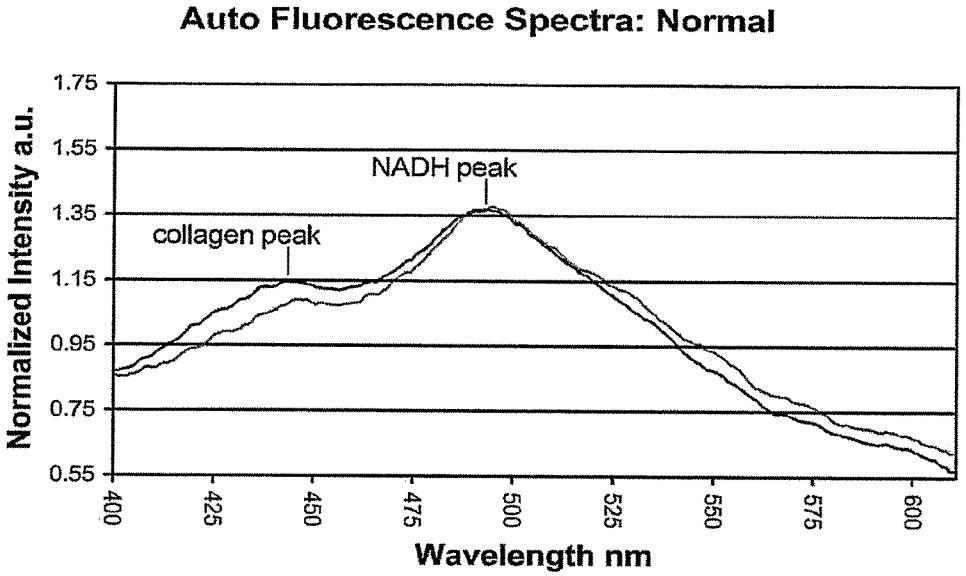

Fig. 27A

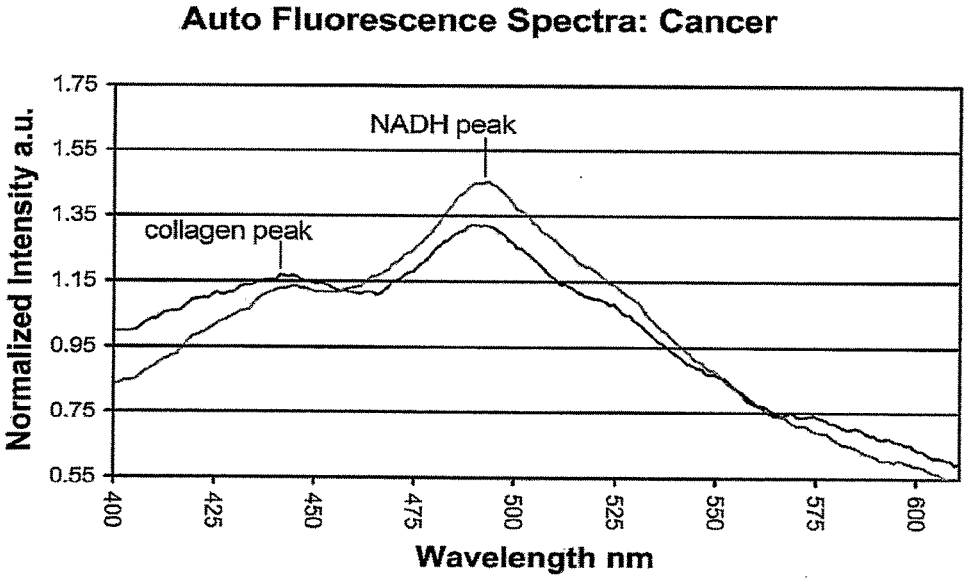

Fig. 27B

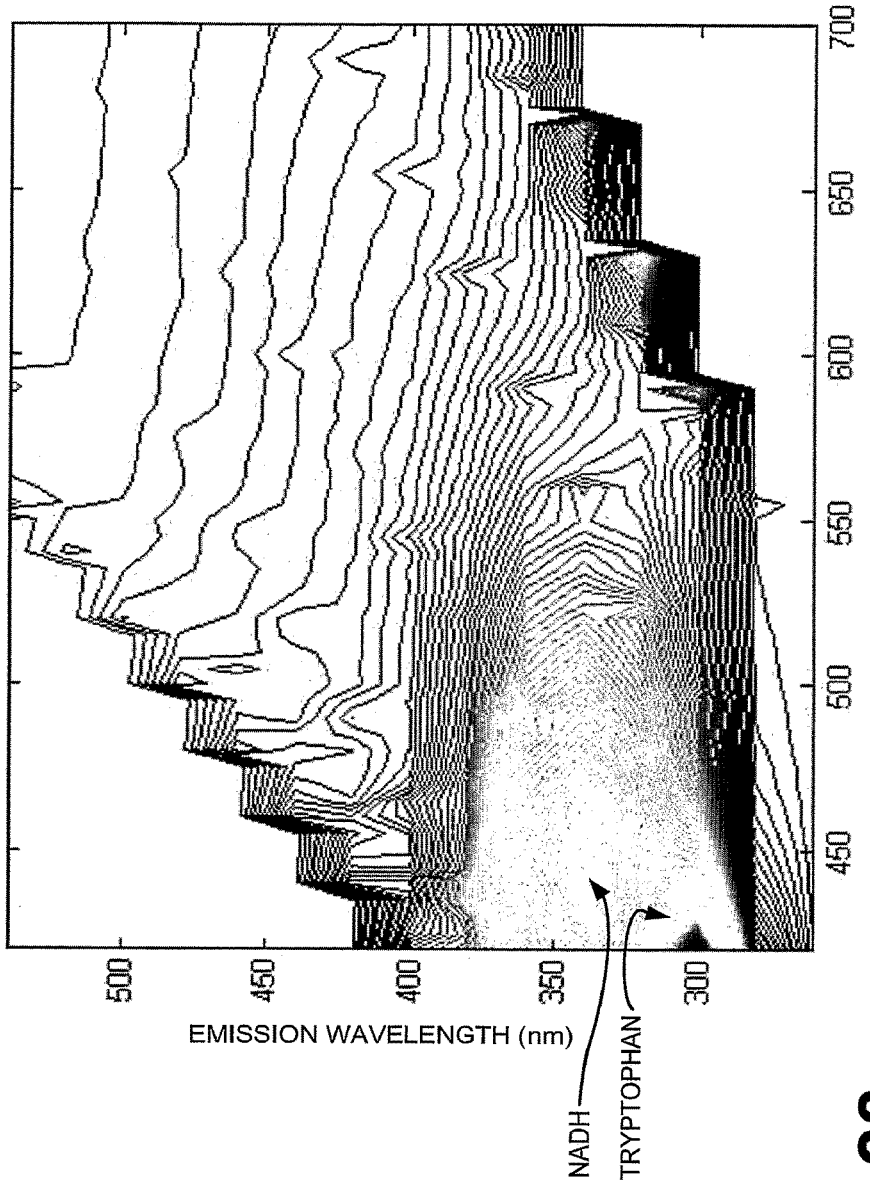
500
450
400
350
300
EMISSION WAVELENGTH (nm)
NADH
TRYPTOPHAN
450
500
550
600
650
700
EXCITATION WAVELENGTH (nm)
CONTOUR PLOT OF EEM MATRIX DATA

Fig. 28

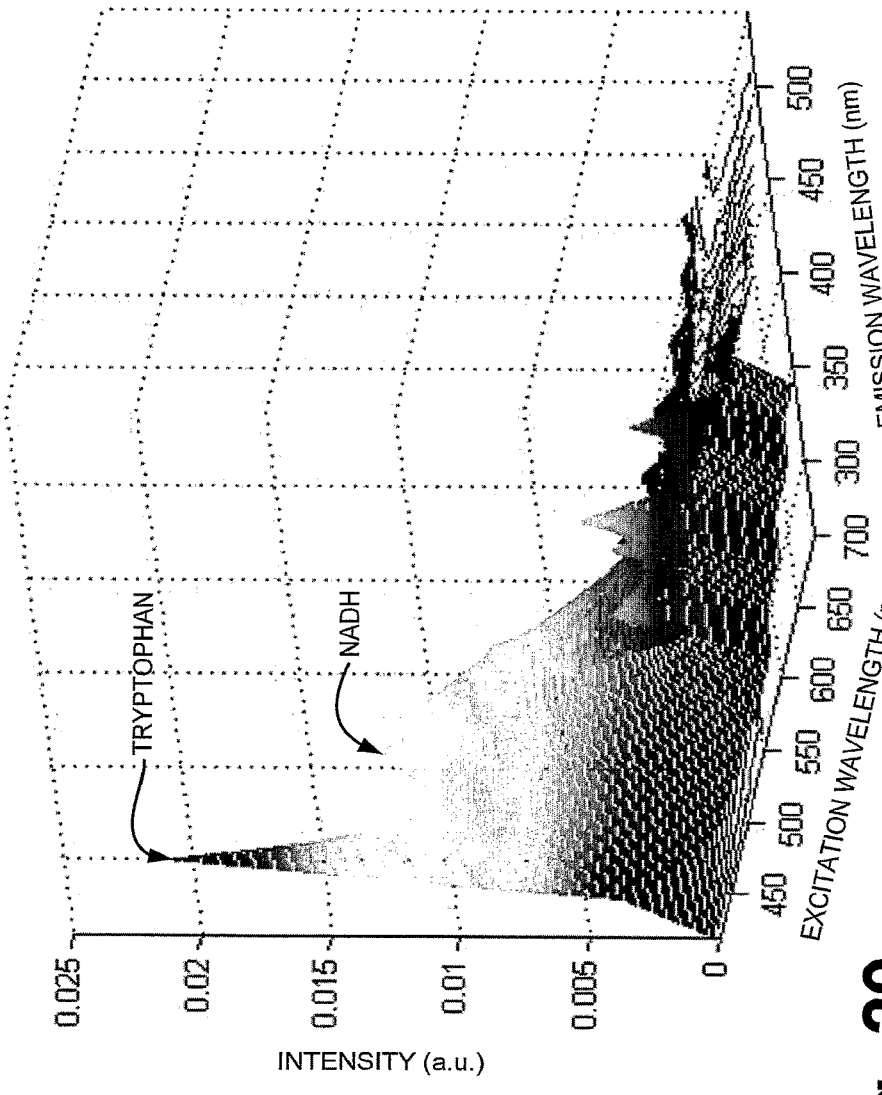

3D PLOT OF EEM MATRIX DATA

Fig. 29

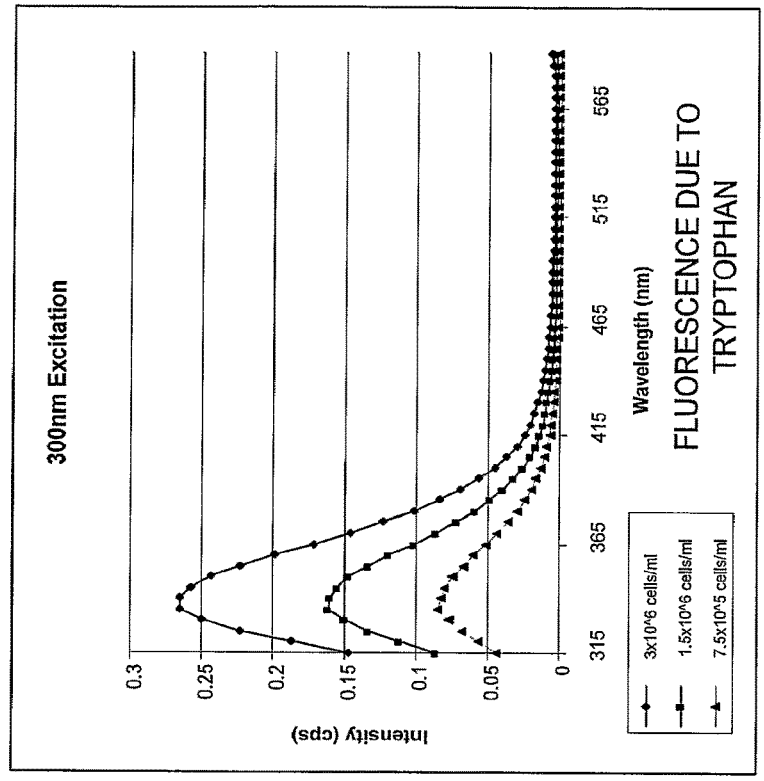

Fig. 30B

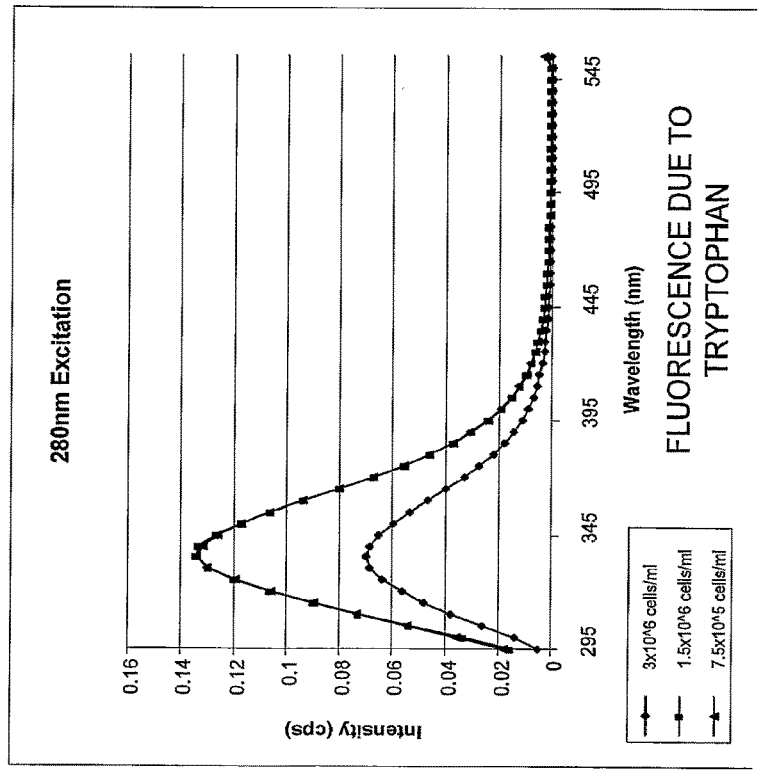

Fig. 30A

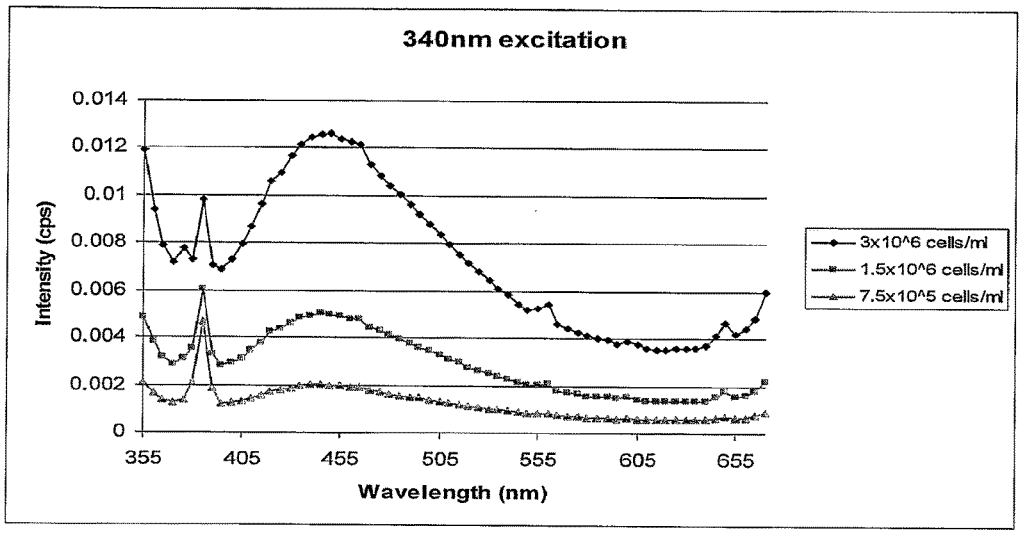

FLUORESCENCE DUE TO NADH at 340nm EXCITATION

Fig. 31A

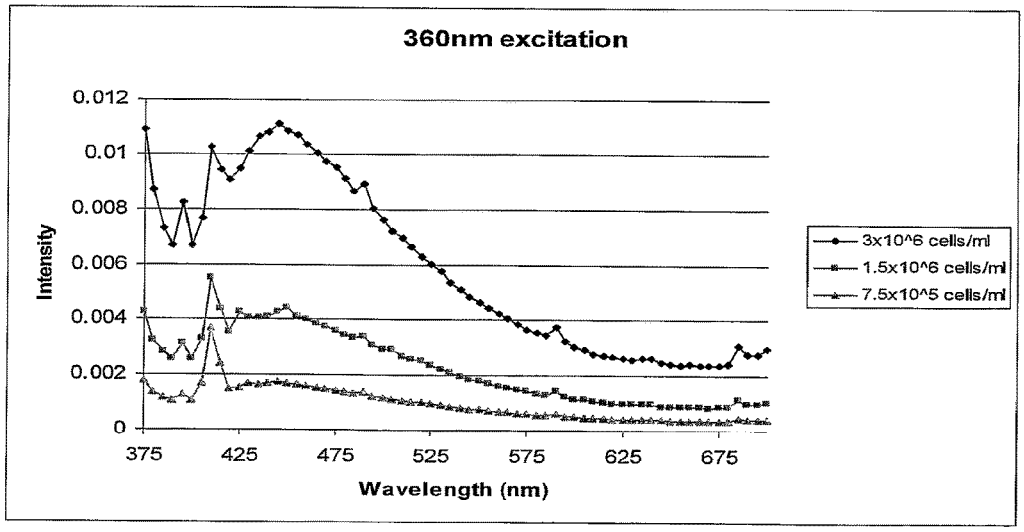

FLUORESCENCE DUE TO NADH at 360nm EXCITATION

Fig. 31B

MULTI-EXCITATION DIAGNOSTIC SYSTEM AND METHODS FOR CLASSIFICATION OF TISSUE

CROSS REFERENCE TO RELATED APPLICATIONS

[0001] This application is a continuation of U.S. application Ser. No. 13/691,067 filed on Nov. 30, 2012, which is a continuation of US National application Ser. No. 11/913,042 filed on Oct. 29, 2007 (U.S. Pat. No. 8,406,858) based on PCT/US06/16587 filed May 1, 2006, which is a non-provisional of, and claims the benefit of the filing date of, each of the following provisional applications, the entire disclosure of each of which is incorporated herein by reference for all purposes: U.S. Provisional Patent Application No. 60/676,420 filed Apr. 29, 2005 and U.S. Provisional Patent Application No. 60/718,194 filed Sep. 15, 2005.

[0002] This application is also related to concurrently filed, commonly assigned, Patent Cooperation Treaty Application No. PCT/US2006/017156, entitled "ELECTROMAGNETIC SYSTEM FOR THE CHARACTERIZATION OF TISSUE," the entire disclosure of which is also incorporated herein by reference for all purposes.

STATEMENT REGARDING FEDERALLY SPONSORED RESEARCH OR DEVELOPMENT

[0003] The U.S. Government has a paid-up license in this invention and the right in limited circumstances to require the patent owner to license others on reasonable terms as provided for by the terms of Grant No. NIH CA66161 awarded by the National Institutes of Health.

BACKGROUND OF THE INVENTION

[0004] This application relates generally to tissue characterization. More specifically, this application relates to methods and systems for using electromagnetic radiation to characterize tissue.

[0005] It is well known that cancer continues to be a highly destructive disease, resulting in large numbers of deaths every year. For example, approximately 30,000 new case of oral squamous cell carcinoma are diagnosed every year, resulting in an annual death rate of this type of cancer itself of about 8000. Current treatments of cancer, whether they be surgical, chemical, or radiological, have a number of complications that can greatly diminish quality of life of patients by themselves. A recognized way to avoid these complications centers around early detection of malignant cells, or of cell properties that are precursors to malignancy. Treatment options are far less invasive and damaging when these conditions are detected early.

[0006] In the case of oral cancer, for example, oral carcinoma is commonly preceded by dysplasia. Dysplastic and cancerous cells differ in their biochemical and morphological properties when compared with healthy cells, and this may, in principle, be used as a mechanism for diagnosis. Currently, such precancerous molecular or chromosomal abnormalities are largely undetectable. In addition, geographic misses frequently occur, leading to false-negative biopsies. Cancers are often multifocal—a positive biopsy at one site may not give a full picture of the extent of the disease if the cancer is multifocal or has extended to "skip areas." Furthermore, there is currently no standard technique for determining genetically abnormal tissue at resection margins in operating rooms. Such abnormalities are clinically undetectable and may lead to recurrence despite complete resection as determined by frozen section.

[0007] Prostate cancer is another example of a multifocal disease characterized by a high prevalence and marked heterogeneity of its morphology and clinical behavior. Prostate cancer remains the most common visceral cancer and the second most common cause of male cancer deaths in the United States. Nearly 1 million men are screened for prostate cancer annually in the United States. In 2006, it is estimated that 234,460 of these men will be diagnosed with prostate cancer and 27,350 will die from this disease.

[0008] Transrectal ultrasound (TRUS) guided needle biopsy is the current standard to diagnose prostate cancer. However, the clinical prostate cancer detection rate of TRUS-guided needle biopsies is only 25-30%, while more than 50% of cancers that require definitive treatment remain undetected during initial biopsies. Such undetected cancers are at high risk of spreading beyond the prostate gland and metastasizing to distant sites. Since prostate biopsies are taken randomly without any knowledge of tissue morphology, they often fail to provide an accurate pathologic/clinical stage of the disease.

[0009] Opportunities to intervene may be enhanced if accurate detection of the predisease/disease state can be achieved at the biochemical, structural, or pathological/physiological level. Presently, there are no real-time diagnostic tools available to assist the urologist in the in vivo detection of tissue abnormalities associated with prostate cancer. While TRUS images can identify prostate borders, the procedure cannot discriminate between benign and malignant prostatic tissue.

[0010] All of these factors contribute to a general need for methods and systems that permit accurate and simple in vivo characterization of tissue.

BRIEF SUMMARY OF THE INVENTION

[0011] Implementations described herein provide methods of characterizing tissue to distinguish between benign and malignant tissue. The tissue is irradiated with light and light scattered and fluoresced from the sample is received. A plurality of distinct excitations of the sample is identified from the received light. On-diagonal components of an excitation emission matrix are identified from the plurality of distinct excitations simultaneously with identifying off-diagonal components of the excitation emission matrix from the plurality of distinct excitations. The excitation emission matrix is accordingly generated from the identified on-diagonal elements and the identified off-diagonal elements. A plurality of spectroscopic measures are derived from the excitation emission matrix and fluorescence spectra, permitting the tissue to be classified according to properties of the derived plurality of spectroscopic measures.

[0012] The tissue may be classified by applying a pattern recognition technique to the derived plurality of spectroscopic measures. Derivation of the plurality of spectroscopic measures may comprise calculating a diffuse reflectance from the diagonal components of the excitation emission matrix. Certain of the spectroscopic measures may be calculated from the diffuse reflectance. Examples of spectroscopic measures that may be derived include a single scattering spectrum, a multiple scattering spectrum, and a

fluorescence spectrum. In some instances, boundary-layer measurements may be removed from the plurality of spectroscopic measures.

[0013] The tissue may be illuminated with light from a plurality of different sources at different wavelengths. In one implementation, at least one of the sources is a broadband light source and another of the sources is bandwidth-limited incident light source in the UV and near UV spectrum.

[0014] In one implementation, a diagnostic software system network is trained to differentiate between benign and malignant tissue. A plurality of spectra is acquired for distinct positions of the tissue. The artificial neural network is then instructed to search for differentiating features of the spectra. Tissue specimens that correspond to the distinct positions are produce and the differentiating features of the spectra determined by the artificial neural network are compared with pathological observations of tissue specimens. Feedback is then provided to the artificial neural network based upon correlations between the pathological observations and the differentiating features.

[0015] In another implementation, morphology of tissue is determined. First, a plurality of spectra for distinct positions of the tissue is acquired. Next, the spectra are observed for distinguishing features to differentiate between benign and malignant tissue. Then each distinct position is defined as at least benign or malignant. A system for determining morphology of tissue may comprise a light source, an optical probe, a spectrometer, a detector, and a computer. A transmitting optical fiber couples the optical probe with the light source and transmits light from the light source to the optical probe. The spectrometer is coupled with the optical probe via at receiving optical fiber. The detector is coupled with the spectrometer and translates optical spectral data from the spectrometer into digital data for processing by the computer. The computer includes a processor and memory and is coupled with and controls each of the light source, the spectrometer, and the detector. An artificial neural network module stored in the memory and executed by the processor. The artificial neural network module is trained to analyze the digital data corresponding to the optical spectral data to differentiate between benign and malignant tissue.

[0016] In another implementation, tissue is spectrally classified. A cell line corresponding to a morphology of the tissue is suspended within a suspension medium. Next, a fluorometric analysis of the cell line is conducted to determine a fluorescence spectrum of the cell line. Then an excitation-emission matrix is produced corresponding to the fluorescence spectrum of the cell line.

[0017] In another implementation, an optical biopsy needle device comprises an elongate biopsy needle with a distal tip and a fiber optic bundle with at least one transmitter fiber and at least one receiver fiber. The fiber optic bundle extends within the biopsy needle and terminates at a distal end at the distal tip of the biopsy needle. The optical biopsy needle device may be used to contemporaneously classify and biopsy tissue. The optical biopsy needle device is connected with a spectral analysis device. The distal tip of the biopsy needle is positioned adjacent to or within the tissue. A spectral response associated with a distinct position of the tissue is obtained. The spectral response is evaluated with the spectral analysis device to determine whether the tissue is normal, benign, or malignant. The distinct position is then biopsied if the tissue is determined to be malignant.

BRIEF DESCRIPTION OF THE DRAWINGS

[0018] A further understanding of the nature and advantages of the present invention may be realized by reference to the remaining portions of the specification and the drawings wherein like reference numerals are used throughout the several drawings to refer to similar components.

[0019] FIG. **1**A is a graph depicting elastic scattering spectra for healthy prostate tissue.

[0020] FIG. **1**B is a graph depicting elastic scattering spectra for cancerous prostate tissue.

[0021] FIG. **2** provides an illustration of fluorescence spectroscopy.

[0022] FIGS. **3**A-**3**C are schematic illustrations of structures that may be used for electromagnetic irradiation of a sample and collection of data;

[0023] FIG. **4** is a schematic illustration of a computational system on which methods of the invention may be embodied.

[0024] FIG. **5** is a block diagram summarizing functionality for implementing methods of the invention in some embodiments.

[0025] FIG. **6** provides an example of the application of the functionality of FIG. **4** to different oral-tissue samples.

[0026] FIG. **7** is a flow diagram summarizing methods for characterizing a sample in accordance with embodiments of the invention.

[0027] FIG. **8** is a schematic diagram of one implementation of a system for spectral analysis of tissue.

[0028] FIG. **9** is a flow diagram of an exemplary calibration method for an optical diagnostic system for tissue classification.

[0029] FIG. **10** is a flow diagram of an exemplary spectral data decomposition method in an optical diagnostic system for tissue classification.

[0030] FIG. **11** is a flow diagram of an exemplary artificial neural network classification scheme for spectra data collected from tissue in an optical diagnostic system.

[0031] FIG. **12** is a schematic diagram of another implementation of a system for spectral analysis of tissue.

[0032] FIG. **13** is a schematic diagram of an embodiment of an excitation unit as depicted in FIG. **12**.

[0033] FIG. **14**A is an isometric view of an in vivo optical probe.

[0034] FIG. **14**B is a left end elevation view of the optical probe of FIG. **14**A.

[0035] FIG. **15**A is an isometric view of an optical biopsy needle.

[0036] FIG. **15**B is an enlarged detail view of a distal tip of the optical biopsy needle as indicated in FIG. **15**A.

[0037] FIG. **15**C is a side elevation view in cross section of the distal tip of the optical biopsy needle of FIG. **15**A as indicated in FIG. **15**B.

[0038] FIG. **15**D is an end elevation view in cross section of a tissue resection feature of the optical biopsy needle of FIG. **15**A as indicated in FIG. **15**C.

[0039] FIG. **15**E is an orthogonal view of the distal tip of the optical biopsy needle of FIG. **12**A as indicated in FIG. **12**C.

[0040] FIG. **16** provides illustrative results using a first sample.

[0041] FIG. **17** provides illustrative results using a second sample.

[0042] FIGS. **18**A and **18**B provide illustrative results using a third sample.

[0043] FIGS. **19**A and **19**B provide illustrative results using a fourth sample.

[0044] FIG. **20** provides a graph of diffuse reflectance extracted from three oral mucosa samples.

[0045] FIG. **21** provides extracted portions of an excitation emission matrix corresponding to data of FIG. **17**.

[0046] FIG. **22** provides an example of a decision hyperplane that may be used for separation of differently characterized tissue.

[0047] FIG. **23** provides a schematic representation of an arrangement used to collect data in certain examples.

[0048] FIGS. **24**A-**24**E provide results of an analysis of a first tissue sample using the arrangement of FIG. **20**.

[0049] FIGS. **25**A-**25**E provide results of an analysis of a second tissue sample using the arrangement of FIG. **20**.

[0050] FIG. **26** is a graph depicting the absorption spectra of both healthy and cancerous prostatic tissue.

[0051] FIG. **27**A is a graph depicting the fluorescence spectra of formalin-fixed, paraffin-embedded, healthy prostatic tissue.

[0052] FIG. **27**B is a graph depicting the fluorescence spectra of formalin-fixed, paraffin-embedded, cancerous prostatic tissue.

[0053] FIG. **28** is a contour plot of excitation vs. emission wavelengths for a DU145 malignant prostate cell suspension.

[0054] FIG. **29** is a three-dimensional plot of intensity vs. excitation wavelength vs. emission wavelength for a DU145 malignant prostate cell suspension.

[0055] FIG. **30**A is a graph depicting the intensity of fluorescence from tryptophan of a DU145 malignant prostate cell suspension upon excitation by light at a wavelength of 280 nm.

[0056] FIG. **30**B is a graph depicting the intensity of fluorescence from tryptophan of a DU145 malignant prostate cell suspension upon excitation by light at a wavelength of 300 nm.

[0057] FIG. **31**A is a graph depicting the intensity of fluorescence from NADH of DU145 malignant prostate cell suspension upon excitation by light at a wavelength of 340 nm.

[0058] FIG. **31**B is a graph depicting the intensity of fluorescence from NADH of DU145 malignant prostate cell suspension upon excitation by light at a wavelength of 360 nm.

DETAILED DESCRIPTION OF THE INVENTION

1. Introduction

[0059] Embodiments of the invention use electromagnetic properties to characterize tissue, with specific embodiments using certain spectroscopic properties recognized by the inventors to include morphological and biochemical information that may be used to characterize tissue. Fluorescence is measured from samples and may result from intrinsic or extrinsic fluorescence. "Intrinsic fluorescence" refers to fluorescence from molecules that occur naturally in a sample while "extrinsic fluorescence" refers to fluorescence from molecules that have been added to the sample by an external mechanism.

[0060] Optical spectroscopy provides a methodology to diagnose disease by quantitatively evaluating changes in tissue morphology and composition. Light interacts with biological tissue in a variety of ways. Various types of tissue fluoresce, absorb, and scatter light in different regions of the electromagnetic (EM) spectrum and by different amounts. The optical properties of tissues are determined by their molecular composition and cellular morphology. Optical techniques utilize accurate measurements of these absorbed or scattered signals to identify benign versus malignant tissues. Based on this principle, optical biopsy techniques have been used to identify various types of surface carcinomas in real-time.

[0061] However, optical properties of different organs are very different. Optical spectroscopic features need to be established for each individual tissue type to provide identification of benign versus malignant tissue. A large majority of scattering events in biological tissue are elastic. Elastic scattering primarily probes morphological features and has proven to be sensitive to cancer grades in several locations.

[0062] FIG. **1**A illustrates the elastic scattering spectra (ESS) of normal prostate tissue. FIG. **1**B illustrates the ESS of malignant prostate tissue. The upper and lower lines in each of FIGS. **1**A and **1**B indicate the upper and lower boundaries of a number of spectral readings obtained from surgically removed prostatectomy specimens of several patients. There is a distinct absorption feature at 580 nm, noticeably greater for malignant tissue than for normal tissue. The shape of this spectral absorption feature is consistent with the absorption spectrum of beta-carotene, a frequent constituent of lipids and cholesterol.

[0063] Another distinguishing spectral feature between FIG. **1**A and FIG. **1**B is the longer-scale slope variations consistent with an increase in the size distribution of the scattering centers for malignant conditions (e.g., nuclei, organelles, etc.). Some of these distinguishing spectral features are consistent with increased perfusion of malignant and pre-malignant lesions. These data indicate that determination of tissue morphology may guide prostate biopsies and direct therapeutic agents in vivo and in real-time.

[0064] Fluorescence spectra may be combined with elastic scattering spectra (ESS) to extend the classification for benign versus malignant tissue. While fluorescence is a weaker process than elastic scattering, it potentially allows for identification of specific endogenous fluorophores whose concentrations may vary with disease state. Analysis of both types of observed signals is therefore desirable. Such analysis may involve estimation of tissue scattering and fluorescence properties, solution of the scattering problem, and prediction of the effect of scattering and absorption on fluorescence signals.

[0065] For purposes of illustration, FIG. **2** shows results that illustrate that fluorescence may be measured on a phantom designed to simulate oral tissue. In this instance, the phantom comprised a light-emitting-diode structure of 200 nm of a proprietary fluorescent material coated on 200 nm of polyethylenedioxythiophene ("PEDOT") coated on an InSnO-coated microscope slide. In addition, FIGS. **27**A and **27**B illustrate fluorescence spectra for normal and malignant prostatic tissue as described in greater detail herein.

2. Data Collection

[0066] An overview of a system that may be used in embodiments of the invention to collect data for analysis is provided with FIGS. **3**A-**3**C. FIG. **3**A shows that at its broadest conceptual level, a sample under test ("SUT") **312**

is evaluated by providing incident light **316** from a source **304** and receiving reflected and/or scattered light **320** from the SUT **312** at a detector **308**. The source **304** may comprise multiple-excitation discrete wavelength pulsed sources spanning a portion of the spectrum, such as by spanning the visible spectrum, and/or may comprise a white-light pulsed source. The detector **308** may comprise a locked detection system.

[0067] A further illustration of the source **304** is illustrated with FIG. **3**B, which shows that light may be generated by an array **326** of sources **324**, which may be substantially monochromatic sources or may be broader-band sources in different embodiments. Examples of light sources **324** include inorganic light-emitting diodes, organic light-emitting diodes, laser diodes, gas lasers, solid-state lasers, fiber lasers, bulbs (halogen, tungsten, xenon, etc.), flash lamps, and the like. It is generally anticipated that different ones of the sources **324** will have different wavelengths or wavelength bands. Operation of the array **326** is controlled by a computational unit **322**.

[0068] Light from the sources **324** may be collimated by a lens **328**, which in some embodiments is an achromatic lens made by combining lenses of glasses having different focal powers so that the light emerging from the lens forms an image substantially free from unwanted colors. The collimated light is spectrally separated with a diffractive element **330** shown in the illustration to comprise a transmissive diffraction grating, but which may alternative comprise a reflective diffraction grating, a prism, or a grism in different embodiments. The spectrally separated light is focused by a lens **332** onto an optical fiber **334** or other type of waveguide, which transmits the light to the SUT **312**.

[0069] A further illustration of the detector **308** is illustrated with FIG. **3**C, which shows that light reflected and scattered from the SUT **312** may be collected with an optical fiber **340** or other type of waveguide and subsequently collimated by a lens **342**. A diffractive element **344**, shown in the drawing as a transmissive diffraction grating, but alternatively comprising a reflective diffraction grating, a prism, or a grism, removes the spectral separation so that a lens **346** may direct the light to an array **348** of detectors **350**. The lens **346** may advantageously again comprise an achromatic lens. Each of the detectors **350** may comprise charge-coupled devices ("CCDs") or other suitable photodetectors, with the computational unit **322** including software to analyze the spectral character of the detected light.

[0070] A structure for the computational device **322** is illustrated schematically in FIG. **4**, which broadly illustrates how individual system elements may be implemented in a separated or more integrated manner. The computational device **322** is shown comprised of hardware elements that are electrically coupled via bus **426**. The hardware elements include a processor **402**, an input device **404**, an output device **406**, a storage device **408**, a computer-readable storage media reader **410***a*, a communications system **414**, a processing acceleration unit **416** such as a DSP or special-purpose processor, and a memory **418**. The computer-readable storage media reader **410***a* is further connected to a computer-readable storage medium **410***b*, the combination comprehensively representing remote, local, fixed, and/or removable storage devices plus storage media for temporarily and/or more permanently containing computer-readable information. The communications system **414** may comprise a wired, wireless, modem, and/or other type of interfacing connection and permits data to be exchanged with external devices.

[0071] The computational device **322** also comprises software elements, shown as being currently located within working memory **420**, including an operating system **424** and other code **422**, such as a program designed to implement methods of the invention. It will be apparent to those skilled in the art that substantial variations may be used in accordance with specific requirements. For example, customized hardware might also be used and/or particular elements might be implemented in hardware, software (including portable software, such as applets), or both. Further, connection to other computing devices such as network input/output devices may be employed.

[0072] FIG. **5** provides a schematic overview of general system signals and data flow used in an embodiment. The light sources are designated at block **504** and may comprise a number m sources used to probe the SUT **508**. Embodiments of the invention result in the generation of an excitation emission matrix ("EEM") and the broader the linewidth of the sources, the fewer the number of matrix elements that can be non-spectrally-overlapping within a given spectral region. The electromagnetic subsystem that delivers the radiation from the sources **504** to the SUT **508** may comprise a guided-wave system or a free-space system. In the case of electromagnetic waveguide delivery, the waveguide may comprise an optical fiber or other type of waveguide as illustrated in FIG. **3**B. The radiation may be delivered to the SUT **508** from a waveguide that employs an aperture such that the evanescent, near-field waves of the waveguide illuminate the SUT **508** or such that the far field of the waveguide illuminates the SUT **508**. The m sources may be combined spatially in a multiplexing system, free space or guided wave, or they may individually illuminate the sample at different locations through the electromagnetic subsystem.

[0073] The radiation **512** from the SUT **508** can be captured by an electromagnetic subsystem such as illustrated in FIG. **3**C. The response of the SUT is first captured by this electromagnetic subsystem, which serves as the front end of an electromagnetic receiver. The purpose of the receiver is then to discriminate the collected electromagnetic radiation into n wavelength intervals of the electromagnetic spectrum. That is, the output of the receiver for a single source input is n (integrated) intensity values, each representing an integral of intensity values over some interval of the wavelength spectrum. The discrimination of the electromagnetic radiation into n integrated intensity values can be accomplished by using numerous methods, including with photodetectors having absorptive filters, spectrometers, and wavelength-selective organic photodetectors.

[0074] The correlation of responses from the SUT **508** with the individual sources **504** may be accomplished using either time-division or space-division multiplexing. In the time-division multiplexing scheme, individual sources are pulsed and the response of the SUT **508** is captured from this region only. The space-division multiplexing scheme may or may not involve the individual control of the sources in different embodiments.

[0075] Additional elements of a data collection system may include light delivery systems and collection probes. Examples of these components are further described below.

3. Data Analysis

[0076] One method of data analysis is described as follows. The matrix characterizing the SUT **404** may generated by the EEM generator **416** in the following manner. If $s_i(\lambda_s)$ is the ith intensity source spectrum (for i=1, 2, . . . , m) and $r_i(\lambda_r)$ is the intensity spectral response of the tissue due to the ith source (for i=1, 2, . . . , n), then the function of input wavelength λ_s (excitation wavelength) and output wavelength λ_r (received wavelength) that may be determined from the radiation **412** collected through the electromagnetic subsystem at the front end of the receiver is

$$X(\lambda_s,\lambda_r)=s_i(\lambda_s)r_i(\lambda_r), \tag{1}$$

where the value of i takes on values from 1 to m, the number of sources. A matrix of values may be formed from this data object by having the receiver perform integrations. The total source power levels are determined from the integrals

$$P_i=\int d\lambda_s s_i(\lambda_s), \tag{2}$$

where the integration interval includes all values at which the source emits power. The emission linewidth of the ith source is denoted $\Delta\lambda_{s_i}$ with the integral being performed over this linewidth. The receiver power levels are determined from integrals over intervals $\lambda_j^{\pm}$ such that the ijth component of the m×n matrix M is given by

$$M_{ij}=\int_{\lambda_j^-}^{\lambda_j^+} d\lambda_r r_i(\lambda_r), \tag{3}$$

where optimal values of $\lambda_j^{\pm}$ may be determined by the experimenter and/or data processor. The source may also be parsed as the output by writing that

$$S_{ij}=\int_{\lambda_j^-}^{\lambda_j^+} d\lambda_s r_i(\lambda_s). \tag{4}$$

Evidently,

[0077]

$$P_i=\sum_j S_{ij}. \tag{5}$$

When a spectrometer is used within the receiver, the intervals $\Delta\lambda_j=\lambda_{j+}-\lambda_{j-}$ can be very fine, for example, as fine as 0.01 nm although spacings of 0.4 nm are also in use, but this example is not intended to be limiting since larger intervals may be used as well. In practice, decisions on tissue characterization may be made on some total number of features N_f that is generally less than 15. In an exemplary system with eight sources, then, at most two output points per source may be of interest. But further processing may advantageously use many more points for stability and identification in the processing algorithm before the task of reducing the EEM to features is performed.

[0078] A square matrix may be generated from the n×m matrix to easily define the elastically scattered terms with the matrix diagonal. A condition on the spectral widths may be exploited to do this: When $\Delta\lambda_{s_i}\geq\Delta\lambda_j$ for all values of i and the values $n_{s_i}\approx\Delta\lambda_{s_i}/\Delta\lambda_j$ are approximated as integers, then

$$n_m\approx\sum_{i=1}^{m} n_{s_i} \tag{6}$$

to define an $n_m\times n_m$ square matrix whose diagonal is nonzero but may include some off-diagonal filling. The matrix M is then considered as square with diagonal elements representing a measure of the scatting and absorption characteristics (elastic scattering elements) of the SUT **508** weighted by the spectral strength of the source in that region. Off-diagonal elements of the matrix represent a measure of higher-order nonlinear processes such as fluorescence. The diagonal is defined by the points that were generated where the λ_j interval covers the source interval. In FIG. **5**, the diagonal elements are denoted by block **520** and the off-diagonal elements are denoted by block **518**.

[0079] Next, the $n_m\times n_m$ matrix may be expanded to generate an $n_c\times n_m\times n_m$ space. An algorithm is applied to the diagonal elements to separate them into n_c components corresponding to various measures of scattering and absorption, while the off-diagonal elements are expanded using the identity operation. Notably, the expansion of the matrix is a completely invertible operation and none of the original information is lost.

[0080] The expansion of the diagonal elements into three components may be accomplished by first generating the diffuse reflectance vector $D(\lambda)$ from the diagonal elements of the $n_m\times n_m$ square matrix M. The diffuse reflectance is denoted in FIG. **5** by block **524** and corresponds to the elastic scattering. The vector may be generated by performing the following operation:

$$D_i(\lambda)=\sum_j \frac{M_{ij}}{S_{ij}}\delta_{ij}. \tag{7}$$

The generation of the $n_m\times n_m$ square matrix with nonzero diagonal elements results from the S_{ij} used in the above equation being nonzero. In a particular embodiment, a number of operations are performed, including reduction of single scattering as indicated at block **532** and separation of the remaining diagonal elements into those that come from absorption as indicated at block **528** and those that are due to multiple scattering as indicated at block **536**.

[0081] The oscillations may be split from the diffuse reflectance by subtracting the windowed average of the diffuse reflectance from the diffuse reflectance:

$$S_i=D_i(\lambda)-\sum_j W_{ij}D_j, \tag{8}$$

where W_{ij} is a window function of width w. From the windowed diffuse reflectance, the remaining two elements may be extracted. This may be performed by noting the following unique features of turbid media such as tissue and absorption spectra. The diffuse reflectance due to multiple scattering contributions from particles smaller than a wavelength is a monotonically decreasing function of wavelength and for the visible region of the electromagnetic spectrum is approximately linear for scattering elements $\Delta na<0.2$ μm, where Δn is taken to be the difference in the index of refraction between the nucleus and the cytoplasm in a cell, which is approximately 0.1. The second element aiding in the separation is the broadening of absorption features for elements in tissue, which generates an imbalance in the first

derivative (divided difference) of the smoothed diffuse reflectance that can be averaged out of the first derivative (divided difference) if the entire absorption feature is captured or can be balanced out of the response using centroids to balance the first derivative. The monotonically decreasing function may then be extracted from the balanced first derivative (divided difference) and subtracted from the smooth diffuse reflectance, yielding the absorption contribution of the tissue response. The monotonically decreasing function and the absorption contribution are the second and third elements of the diagonal expansion.

[0082] The new $3\times n_m\times n_m$ space generated by the expansion of the matrix characterizing the tissue may be reduced to a number of features that are independent to enable classification of the signature from this array of digitally filtered input data. There are numerous automated techniques known to those of skill in the art for estimating the number of terms that could be used for attempting to recognize a data pattern. When too many factors are used, the recognition becomes non-unique; when too few are used, the recognition cannot be made. In embodiments of the invention, the spectral broadening in the tissue may place a limit on the minimum meaningful spectral width of a feature to be used. The inventors have found in certain investigations that this minimum is generally on the order of 30-50 nm, but identification of this value is not intended to be limiting. The diagonal of the square matrix may then be reduced to factors by summing over diagonal elements, whereas as a whole off-diagonal elements can be used in a similar manner.

[0083] A common term for methods that find the number of independent features from each data sample is "principal component analysis." When many tissue samples are lumped together such that there are $N_{samples}\times n_c\times n\times m$ arrays processed simultaneously, the techniques are often called "multispace techniques." Here, single-data-point techniques are those that are used. Once the data have been reduced to N_f independent values such that the problems may be considered to be an identification problem in an N_f-dimensional space, permitting any of several pattern-classification techniques known to those of skill in the art to be implemented by the pattern classifier **440** to classify the result into one of $N_{patterns}$. The pattern-classification techniques may be used generally to separate the N_f-dimensional space by (N_f-1)-dimensional hyperplanes and find in which box the data point resides.

[0084] An illustration of the approach described above to squamous cell carcinoma is illustrated in FIG. **6**. The structure of FIG. **6** generally parallels the structure of FIG. **5**, with the results for the EEM of block **516** being denoted **604**, the off-diagonal elements of block **518** being denoted **612**, the diffuse reflectance of block **524** being denoted **608**, the single scattering of block **532** being denoted **620**, the multiple scattering of block **528** being denoted **616**, and the absorption of block **536** being denoted **624**.

[0085] The methods described above are summarized with a flow diagram in FIG. **7** that identifies specific steps that may be performed in implementations of methods of the invention. Data from a sample are collected by irradiating the sample with light at block **704** and receiving light scattered from the sample at block **708**. Multiple distinct excitations of the sample are identified from the received light at block **712**, which permits on-diagonal components of the EEM and off-diagonal components of the EEM to be identified simultaneously at block **716** using the techniques described above. The EEM is generated at block **720** from the identified components.

[0086] Once the EEM has been generated, it may be used at block **724** to derive a plurality of spectral measures, which in one embodiment include absorption, fluorescence, multiple scattering, and single scattering. The group of measures is used for each point within a spatial distribution to generate a contour plot of the sample at block **728**. For example, in embodiments where the sample is tissue disposed on a slide, the contour plot may correspond to the spatial distribution of the slide. The contour plot may subsequently be processed at block **732**. Such processing may remove extraneous information, such as by removing glass and boundary-layer measurements from tissue measurements when the sample has been prepared on a glass slide. Such removal may be accomplished with a cluster-analysis program in one embodiment, or with a generic filter that examines the fluorescence and scattering to remove data points identified as corresponding to boundary points or glass points in another embodiment.

[0087] As indicated at block **736**, the spectral measures may then be used to classify the sample. In one embodiment where the sample comprises biological tissue, this is performed with a cluster analysis that separates the tissue into three categories—"normal," "dysplastic," and "cancerous." Such cluster analysis may group together items using a statistical analysis of a Euclidean distance measure in three-space generated with the fluorescence, scattering, and absorption measures.

[0088] Other methods of data analysis may include principal component, artificial neural networks (ANN), and various statistical analyses that may be employed to develop a preliminary classification scheme for in vivo diagnosis of tissue. For example, classification of ESS may be performed in a binary classification scheme using an ANN. Other alternatives include the use of logistic regression, Gaussian processes, and support vector machine algorithms to improve the classification scheme.

4. Diagnostic Devices

[0089] In one implementation, an optical probe device and techniques for diagnosis may be utilized on patients suspected of having prostate carcinoma due to an elevated serum prostate-specific antigen (PSA) and/or abnormal digital rectal exam (DRE). Instead of randomly investigating a patient's prostate by taking multiple biopsy samples, an optical probe mounted at the tip of the biopsy needle (i.e., an optical biopsy needle) may be used to explore the morphology of the prostate before extracting a tissue sample. By first conducting optical measurements, areas of carcinoma, dysplasia, or other cellular abnormalities can first be discovered to inform the locations for taking a tissue sample. A combination of ESS and fluorescence measurements may be used to determine tissue scattering properties and measure relative concentrations of fluorophores in the tissue. These optical measurements may then be compared with standard histology on the tissue sample taken to predictively determine disease state.

[0090] FIG. **8** depicts an exemplary system **800** for performing in vivo or ex vivo optical diagnostics of prostate tissue. The system **800** may include an optical probe **802** (for example, a stand-alone device or an optical probe mounted within a biopsy needle or a cryoprobe), which contacts the

prostatic tissue **814**, a light source **804**, a bandpass filter **806**, a spectrometer **808**, a detector **810**, and a computer **812**. The light source **804**, the bandpass filter **806**, the optical probe **802**, the spectrometer **808**, and the detector **810** may each be connected in turn via fiber optic cabling. The computer may control each of the light source **804**, the bandpass filter **806**, the spectrometer **808**, and the detector **810**.

[0091] For elastic scattering, the light source **804** may be an Ocean Optics LS-1 Tungsten/Halogen light source and the spectrometer **808** may be an 52000 double spectrometer. The detector is generally a charge coupled device (CCD) array, which may be integral with or separate from the spectrometer **808**. While a Tungsten/Halogen source offers the ability to generate an EEM that can yield information concerning scattering and absorption, such broadband sources hide fluorescent signals and cannot be modulated at a sufficient rate to yield any information that will aid in the determination of the absorption coefficient.

[0092] For fluorescence, a variety of available light sources **804** may be used including, for example, a Varian mercury arc lamp and several LED sources. In some implementations the light source **804** may provide a pulsed light output. A Jarrell Ash ¼ m monochromator may be coupled with the light sources **804** as the bandpass filter **806** for wavelength selection. Detection may be accomplished using a Princeton Instruments intensified CCD array detector as the detector **810** coupled with an Acton 300i ⅓ m Imaging Spectrometer as the spectrometer **808**.

[0093] The light source **804** generates steady or pulsed light that is filtered into discrete bandwidths by the bandpass filter **806** before being output to the optical probe **802**. The optical probe **802** is used to make elastic scattering and fluorescence excitation-emission measurements at different locations on the prostate. The elastic scattering and fluorescence spectra received at the optical probe **802** are transmitted to the spectrometer **808** and then passed to the detector **810**. The data output from the detector **810** is transmitted to the computer. Once the data is stored, it is arranged in a database that is processed using an ANN program or other appropriate analytical software.

[0094] One programming language that may be utilized for data collection, data processing, and for mathematical programming is Mathematica (Wolfram Research). Morphological data of prostate pathology extracted from the optical probe may include characterization of tissue as benign versus malignant and characterization of aggressiveness of the malignancy according to the Gleason sum or as low/medium/high grade.

[0095] The computer may execute Diagnostic Spectroscopy Software (DSS) to analyze the optical data returned by the probe **802**, spectrometer **812**, and detector **814**. DSS utilizes photon migration theory for classification of biological tissue. Multiple sources with limited wavelength range and different center wavelengths are used by the DSS to determine a spectral response of tissue over a broad continuous wavelength range. Resulting spectra from multiple excitation sources may be separated into different types of light-tissue interaction mechanisms.

[0096] The DSS does not rely on single feature identifications because a single marker of a condition may not always evolve with the condition in exactly the same sequence or in exactly the same manner. Instead, the DSS monitors a number of different spectral features and their collective evolution simultaneously to increase the probability of an accurate diagnosis. The DSS may utilize any set of excitations that cover the wavelength range of interest and a DSS spectral decomposition does not require detailed tissue models. Therefore, the DSS may be used to generate an EEM, for example, as described herein above and in the examples below. Based only on the data taken, EEMs may be decomposed into auto-fluorescence spectra (AFS), tissue absorption spectra (TAS), ESS, and cell distribution spectra (CDS). These spectra can be used in conjunction with an ANN, logistic regression, or similar methods to develop an overall DSS classification scheme. The decomposed spectra may be used, for example, to train the ANN for the diagnosis of prostatic cancers and the model may be inverted for use as a diagnostic tool.

[0097] Information about a given sample in a DSS classification is not only spread across the spectrum, but also into separate and distinct spectra that are mathematically independent due to different causative events. Cancer detection requires comparison of samples of healthy tissue with pre-malignant and malignant samples. Thus, the relative changes are more important than absolute values, as they may vary strongly from subject to subject.

[0098] FIG. **9** illustrates an exemplary calibration method for a diagnostic system including an optical probe and DSS. A fiber optic probe (as described above in FIGS. **8** and **9** and in greater detail below with respect to FIGS. **14**A-**15**E) and the DSS are calibrated for background fluorescence, reflectance and as well as for throughput prior to EEM data generation. The process of calibration begins with operation **902** wherein any control and data files in the system (e.g., in the spectrometer **808** or other components in FIG. **8** or the excitation unit **904** of FIG. **12** as described below) that are used to diagnose prostatic tissue being uploaded in the computer implementing the DSS are calibrated. In operation **204** the system is calibrated for background characterization. The probe (e.g., mounted inside the tip of a biopsy needle as described below with respect to FIGS. **15**A-**15**E) is inserted into the prostate and spectroscopic tests identical to EEM data generation are carried out with all light sources turned-off. This enables background subtraction from tissue spectral data while the measured background is insignificant. This subtraction is performed to ensure thoroughness and consistency.

[0099] Next, in operation **906**, the system is calibrated with a reflectance standard, for example, by using a white light standard such as Spectralon. In operation **908**, the system is calibrated with a fluorescence standard (e.g., using Rhodamine B). Next, in operation **910** the background fluorescence is removed, e.g., by subtracting any background fluorescence. In operation **912**, collected spectral data are normalized to a known peak fluorescence at a specific wavelength (e.g., Rhodamine B peak fluorescence intensity at 575 nm) to correct for variations in throughput of the probe and other components of the system.

[0100] FIG. **10** illustrates details of an exemplary implementation **1000** of DSS spectral data decomposition. To limit the time that is required to collect and analyze spectral data in clinical settings, the DSS decomposes spectral data using a set of rules. According to the exemplary methodology of FIG. **10**, spectral data is first converted by the DSS in operation **1002** to an EEM and then decomposed in operation **1004** by separating off-diagonal from diagonal components, rapidly-varying from slowly-varying components, and absorption from scattering. In one example, the

spectral components AFS, TAS, ESS, and CDS described above are separated by the identification of intrinsic versus extrinsic components. The EEM obtained in operation **1002** is thus diagonal within the spectral width of the source. The off-diagonal elements existing outside of the spectral width of the source in the EEM illustrate fluorescence from the sample for a given excitation. The AFS obtained in operation **1004** is the non-diagonal portion of the EEM.

[0101] The diagonal elements are then separated from the EEM. In operation **1006**, the CDS, which is the high frequency component of the diagonal of the EEM, is separated. The low frequency component of the diagonal is then separated, in operation **1008**, and is used to determine both the TAS, by determining the absorption contribution to the low frequency diagonal elements in operation **1010**, and the ESS, by determining the elastic scattering contribution to the low frequency diagonal elements in operation **1012**. There are numerous ways in which to effect this separation. The components of the diagonal EEM elements, absorption coefficient, the non-diagonal elements, and other information are then collected into a file in operation **1014**. The data of this file is analyzed in operation **1016** by comparison to a database of spectra and classified as normal or malignant in operation **1018**. Various modifications, particularly in the order of operations, may be made to operations presented in FIG. **10**.

[0102] FIG. **11** illustrates an implementation of an exemplary ANN classification scheme **1100** for spectra collected from tissue in an optical diagnostic system. The process of ANN classification begins with data reduction and normalization in operation **1102**. Spectral data in the relational database is reduced and normalized. For example, the lowest amplitude observed in the entire population may be subtracted from each data point. Normalized amplitude values may be obtained by dividing the amplitudes by the mean amplitude calculated across each specific case. The final data set may be composed of mean amplitudes over a preset wavelength range, thus condensing the data points into a more manageable representation.

[0103] Next, in operation **1104**, a suitable classification scheme may be selected. For example, a simple binary classification scheme may be employed to classify benign versus malignant prostatic tissue. A two-dimensional array of data may be used in a standard three-layer, back-propagation network. Logistic regression, Gaussian processes, and support vector machine algorithms may also be used to improve the classification scheme.

[0104] The ANN classification scheme **1100** may next select test parameters in operation **1106**. For example, a cancerous tissue classification scheme may be used to predict a minimum of two possible outcomes (benign versus malignant), and may incorporate parameters for cancer grade, tumor size, or tumor density in the model.

[0105] In operation **1108**, the ANN classification scheme **1100** may select diagnostic thresholds. Exemplary diagnostic thresholds may be sets of values of the diagnostic parameters for AFS, TAS, ESS, CDS, and overall DSS classifications that determine the diagnostic outcome, e.g., no cancer, cancer, or cancer grade. A set of values for diagnostic thresholds may be determined based on the ability to properly predict the outcome compared to standard medical diagnostic measures. These diagnostic thresholds are dependent upon sensitivity, specificity, positive predictive value, negative predictive value, and test efficiency for the diagnostic parameters.

[0106] FIG. **12** depicts an alternate embodiment of a system **1200** for optical detection of tissue pathology, wherein an excitation unit **1204** takes the place of the light source **804** and bandpass filter **806** of FIG. **8**. The system **1200** includes, as before, an optical probe **1202**, which contacts the prostatic tissue **1214**, a spectrometer **1208**, a detector **1210**, and a computer **1212**. The system may also include a fiber splitter **1206** that collects the discrete output from the excitation unit **1204** and directs the output to one or more transmitter fibers in the optical probe **1202** as further described below. The excitation unit **904**, the fiber splitter **1206**, the optical probe **1202**, the spectrometer **908**, and the detector **910** may each be connected in turn via fiber optic cabling. The computer may control each of the excitation unit **1204**, the spectrometer **1208**, and the detector **1210**.

[0107] FIG. **13** depicts an exemplary embodiment of the excitation unit of FIG. **12**. The excitation unit **1300** consists of an array of surface mount light emitting diodes (LEDs) **1310** capable of excitation at different wavelengths. The LEDs in the excitation unit may individually controlled by the computer through an input port **1304** that directs control circuitry **1302** within the excitation unit **1300**. The excitation unit **1000** and the control circuitry **1302** therein may be powered via a power input **1306** coupled with an AC/DC converter **1308**. The LEDs **1310** may be coupled with optical fibers **1314** via focusing lenses **1312** for output of light to the optical probe. An exemplary optical fiber may be a Super Eska SH4002 multimode plastic fiber, which has a 1.0 mm core diameter made of polymethyl-methacrylate (PMMA) with a 1.0 mm cladding made of a fluorinated polymer. The numerical aperture (NA) of the fiber is 0.5 and the loss of the fiber is 190 dB/KM. The fiber is protected by a black polyethylene jacket giving the fiber a total of 4.0 mm diameter.

[0108] The emission spectrum of the LEDs **1310** in the excitation unit **1300** may have wavelengths ranging from approximately 450-650 nm. The axial intensity of the LEDs **1310** may be, for example, 160 mcd, which is approximately 3 mW at 550 nm into 4π steradians with a forward current of 20 ma. Other excitation units may, for example, employ LEDs with axial intensities of 1600 mcd as well as modulation circuitry to aid in the determination of the absorption coefficient of the tissue. The LEDs **1310** in the excitation unit **1300** may be easily interchanged to facilitate measurement of any desired wavelength range. The receiving fibers may be connected to a spectrometer for spectral analysis.

[0109] The system is useful for in situ, real-time diagnosis and identification of prostatic carcinomas. In one embodiment, an optical scanning probe **1400** as shown in FIGS. **14**A and **14**B may be used to investigate prostate tissue. As shown, the probe **1400** is primarily composed of a tubular shaft **1402** terminating distally with a distal tip **1406**. The tubular shaft **1402** is preferably 1 cm or less in diameter. However, the diameter of such a probe may vary depending on choice of material, and the wall thickness necessary to withstand pressures and stress levels within the rectal cavity.

[0110] The tubular shaft **1402** houses a plurality of optical fibers **1410** that protrude through an outer end wall **1408** of the tubular shaft **1402** at the distal tip **1406** such that the distal ends of the optical fibers **1410** are flush with the end wall **1408** of the tubular shaft **1402**. The optical fibers **1410**

extend proximally through the tubular shaft **1402** to a proximal cap **1412**, which joins a cable **1404** to the tubular shaft **1402**. The cable **1404** provides sheathed protection to the optical fibers **1408** as they extend proximally from the probe **1400** to connect the probe **1400** to attached analytical equipment, for example, a spectrometer.

[0111] In one implementation, the probe **1400** design comprises fourteen fibers as shown in FIGS. **14**A and **14**B, which include twelve transmitter fibers **1414** distributed about the perimeter of the end wall **1408** and two detector fibers **1416** positioned adjacent the center of the end wall **1408**. Arrangement of the fibers **1410** may be varied and numbers of each of the transmitter fibers and receiver fibers can be greater or lesser. The output of a light source may be routed to the probe **1400** and controlled by the control circuitry, for example, as shown in FIGS. **8**, **12**, and **13**. The transmitter fibers **1414** may thus be illuminated collectively or individually, in sequence or in groupings, and the detector fibers may be read.

[0112] An optical scanning procedure for the diagnosis of prostate cancer and periodic follow-up evaluation of the prostate gland may be performed using the probe **1400** of FIGS. **14**A and **14**B. Measured spectra provide a gross overview of a large volume of tissue, allowing for easier and faster scanning of the entire prostate gland. This information can be utilized in several different ways to manage the disease: 1) to guide prostate needle biopsies to morphologically adverse locations; 2) to provide comprehensive information during radical prostatectomy surgery regarding tumor margins, particularly capsule perforation and local metastasis; 3) to deliver therapeutic agents directly to prostatic cancer foci; and 4) to monitor the response to various therapeutic modalities. Some specific clinical applications include prostate biopsies, brachytherapy, cryotherapy, detection of residual and recurrent disease.

[0113] Sufficient depth of light penetration (2-4 cm) and a wide field of view for the probe **1400** are obtained by selecting source fibers with small numerical apertures (NA<0.2) and receiver fibers with high numerical apertures (NA>0.5). Intensity modulation of the sources and homodyne demodulation at the output of a fast spectrometer may be used to estimate phase and amplitude variations. The phase and amplitude modulations are then used to determine both the scattering coefficient and the location of a lesion responsible for a scattering event.

[0114] In another embodiment, a minimally invasive automatic optical biopsy needle **1500** as shown in FIGS. **15**A-**15**E is used in the diagnosis of prostate cancer. An optical biopsy needle **1500** incorporates an integrated optical probe. The invasive optical biopsy needle **1500** may be designed to capture ESS and fluorescence spectra of prostatic tissues in the range of 200-1,150 nm. The optical biopsy needle **1500** is composed primarily of a long outer sheath **1502** attached to an actuator handle **1504**. The outer sheath **1502** houses an inner needle **1510** (see FIGS. **15**B and **15**C) that is actuated by the actuator handle **1504**. A cord sheath **1508** extends proximally from the actuator handle **1504** to couple the optical biopsy needle **1500** to analytical equipment as further described below.

[0115] The distal tip **1506** of the inner needle **1510** forms and angled blade **1524** to assist in the ability of the inner needle **1510** to puncture through tissue. Initially, the inner needle **1510** is substantially housed within the outer sheath **1502** with only the angled blade **1524** extending beyond the distal end of the outer sheath **1502**. The actuator handle **1504** causes the inner needle **1510** to extend distally from the distal end of the outer sheath **1502** to collect a tissue sample **1522** in the standard manner of biopsy needles. The inner needle **1510** defines a recessed tray area **1516** defined by low sidewalls **1518** spaced proximally from a distal tip **1506** of the inner needle **1510**. The inner needle **1510** also defines a barb **1520** at the top surface of the inner needle **1510** at the distal end of the recessed tray area **1516** extending proximally toward the recessed tray area **1516**. The barb **1520** assists in extracting and securing a tissue sample **1522** within the recessed tray area **1516**. A typical tissue core sample **1522** may be approximately 15 mm long for each biopsy.

[0116] The inner needle **1510** may be engineered to bring a plurality of optical fibers **1512**, **1514** from the actuator handle **1504** to the distal tip **1506** flush with the blade **1524** surface as shown in FIGS. **15**C-**15**E. In one exemplary embodiment, a 16-gauge outer sheath **1502** may house a 20-gauge inner needle **1510**. Three 100-200 μm fibers, one transmitter fiber **1514** and two receiver fibers **1512** may be threaded through conduits formed within the inner needle **1510**. Other embodiments may incorporate needles and sheaths of greater or lesser gauge or alternate numbers and diameters of fibers. Excitation of tissue is preferably restricted to the sample point. A small numerical aperture (circa 0.2 or less) may be used for the transmitter fiber **1514** to ensure that the excitation does not spread too much over the propagation distance. Larger numerical apertures are preferably used for the receiver fibers **1212** in order to maximize the pick-up.

[0117] As shown in FIG. **15**D, the optical fibers **1512**, **1514** travel underneath the recessed tray area **1516** to the distal tip **1506** of the inner needle **1510**. The terminal ends of the optical fibers **1512**, **1514** are positioned flush with the blade surface **1524** of the inner needle **1510** and are exposed therein. The terminal ends of the optical fibers **1512**, **1514** may be spaced apart about the blade surface **1524**. In an exemplary embodiment as shown in FIG. **15**E, the optical fibers **1512**, **1514** may be arranged in a vertical row with the transmitter fiber **1514** flanked above and below by receiver fibers **1512**. Other patterns of arrangement for the optical fibers **1512**, **1514** are possible and greater or fewer fibers may be used. The optical fibers **1512**, **1514** extend proximally through the inner needle **1510** and the actuator handle **1504** and exit the actuator handle **1504** through the cord sheath **1504**. The cord sheath **1508** provides protection to the optical fibers **1512**, **1514** as they extend proximally from the actuator handle **1504** to attached analytical equipment, for example, a spectrometer.

[0118] In actual practice, the optical biopsy needle **1500** may be inserted into the prostate gland at the desired location and signal normalization performed before activating the light source. The distal tip **1506** of the inner needle **1510** is positioned inside the prostate. The receiver fibers **1512** collect the diffuse reflectance and fluorescence emissions from the tissue under excitation generated by the transmitter fiber **1514**. Fluorescence and reflectance measurements are then taken to determine whether the adjacent tissue is benign or malignant. Tissue sample collection may thus be limited to areas of tissue that appear to be abnormal based upon spectral analysis. This procedure is repeated each time and biopsy samples will be taken from several locations of the prostate.

[0119] The presence of blood may restrict the collection region to a fairly thin layer next to the tissue surface. A strategy for limiting the range of excitation may be to choose a spectral range where the signal does not propagate too far into the material, yet still has a large enough scattering coefficient in order to return some signal. The spectral range is selected with particular attention to the absorption coefficient where it will be appreciated that the scattering coefficient does not vary appreciably with wavelength from visible to near infrared (NIR). The absorption coefficient, however, does. Absorption is much larger in the near UV and the blue than in the red and NIR. Higher absorption leads to higher fluorescence that contains more usable information. Therefore, a suitable wavelength range may be in the visible range with one or more excitation signatures below 400 nm.

5. Examples

[0120] The above-described techniques have been tested on a number of different samples, the results for which are summarized in FIGS. **16**-**19**B.

a. Example 1

[0121] Results are provided in FIG. **16** for application of the above-described method to a sample of white wax. Wax has a consistency similar to that of biological tissue. The samples were prepared by coating slides with the wax, with the thickness estimated to be on the order of fractions of a millimeter. The results are presented as four plots, showing the diffuse reflectance, absorption, and multiple and single scattering functions as determined from the diffuse reflectance. In this instance, the fluorescence was negligible.

b. Example 2

[0122] Results are provided in FIG. **17** for application of the above-described method to a sample of red wax. Again, the samples were prepared by coating slides with the wax, with the thickness estimated to be on the order of fractions of a millimeter. The results again show the diffuse reflectance, absorption, and multiple and single scattering functions as determined from the diffuse reflectance.

c. Example 3

[0123] Results are presented in FIGS. **18**A and **18**B for a 10-μm-thick layer of prostate tissue preserved in formalin and mounted in paraffin. FIG. **18**A shows the measured fluorescence and FIG. **18**B shows results after application of the above-described methods, namely the diffuse reflectance, absorption, and multiple and single scattering functions as determined from the diffuse reflectance.

d. Example 4

[0124] Results are presented in FIGS. **19**A and **19**B for a cucumber sample having a thickness believed to be on the order of fractions of a millimeter. Cucumber is much like human tissue except that the cell walls are thicker. FIG. **19**A shows the measured fluorescence and FIG. **19**B shows the results for the diffuse reflectance, absorption, and multiple and single scattering functions. Three fluorescent lines are evident in the results of FIG. **19**A and are believed to correspond to collagen, NADH, and chlorophyll (in the red portion of the spectrum).

e. Example 5

[0125] The fifth example provides results derived from application of the above-described methods and systems on three different types of oral mucosa fixed in formalin and mounted in paraffin in 20-μm sections onto standard microscope slides. Three different slide classifications were made, based on the condition of the oral tissue on the slide: hyperkeratosis, dysplastic, and squamous cell carcinoma. In the results presented in FIGS. **20**-**22**, discussed in detail below, these classifications are identified by the letters "H," "D," and "SCC" respectively. The tissue slides were placed in an optical mount and a probe was used to excite the tissue electromagnetically as described above, and data were collected.

[0126] The EEM generated from each tissue sample was broken up into diagonal and off-diagonal elements as described above, and the diffuse reflectance obtained from the diagonal elements. The diffuse reflectance generated by each of the three different tissue samples is illustrated in FIG. **20**. The off-diagonal elements for the samples are illustrated with the other information extracted from the diagonal elements in FIG. **21**. The diffuse reflectance from the diagonal elements of the EEM was processed further to separate out the single scattering contribution SSS, the multiple scattering contribution MSS, and the absorption. The three elements extracted from the diagonal, along with the off-diagonal elements of the EEM for each tissue sample, are illustrated in FIG. **21**.

[0127] From FIG. **21** it is clear by visual inspection for this example that there are between one and three features that can be used in the decision space to distinguish between hyperkeratosis and the other two classifications. The primary features that can be differentiated are the overall integrated levels of the MSS, fluorescence, and absorption characteristics. These characteristics may be used to form a multidimensional space, in this particular instance a three-dimensional space, with features in the plane defining discriminatory aspects of the characteristics. In particular, for this example, FIG. **22** shows such a space, with a plane drawn in the plane that separates the hyperkeratosis case from the others.

[0128] While this example permits the decision plane to be determined from visual inspection of the elements separated from the EEM, this may not be true generally, particularly in instances where more samples are processed and the number of characteristics is larger. In such instances, embodiments of the invention may use principle constituent analysis and pattern-recognition techniques to determine the decision space and the decision hyperplane.

f. Example 6

[0129] The sixth example provides results of automated tissue classification. The data were collected and analyzed using a system represented schematically in FIG. **23**. The system **2304** uses a probe to acquire spectral data from a non-stained **20**-μm sample of tissue **2308** and a microsocpe imaging system for obtaining images of a region with a 5-μm hematoxylin and eosin stained slide **2312**. The image **2316** is used to generate an EEM using the methods described above in connection with FIG. **6**. The application of cluster programs to the spectral measures derived from the EEM permits classification of the image to generate a decision

map **2320** that characterizes a spatial region of the complete image **2324** as having normal, dysplastic, or cancerous tissue.

[0130] One illustration for these results is provided in FIGS. **24**A-**24**E. FIG. **24**A provides a micrograph of the tissue sample, delineating healthy and cancerous regions. Results of the application of the method of FIG. **6** to this tissue sample are provided in FIGS. **24**C-**24**E to show maps of the absorption, scattering, and fluorescence respectively. FIG. **24**B shows the decision map that results from the classification of the tissue after performing the cluster analyses. Measurements were made using a probe having a plurality of 400-μm fibers to provide a total probe diameter of 1200 μm. Cancerous tissue is identified in the decision map by white regions, with grayscale regions identifying dysplastic and normal tissue. The presence of cancerous tissue in the cancerous region is confirmed by the analysis.

g. Example 7

[0131] The seventh example provides results similar to those of FIGS. **24**A-**24**E and also result from application of the method of FIG. **6** using the system of FIG. **23**. FIGS. **25**A-**25**E have a layout similar to that of FIGS. **24**A-**24**E, with FIG. **25**A providing a micrograph of the sample that delineates healthy and cancerous regions, FIG. **25**B providing the decision map that results from application of the method, FIG. **25**C providing a map of the absorption determined from the EEM, FIG. **25**D providing a map of the scattering determined from the EEM, and FIG. **25**E providing a map of the fluorescence determined from the EEM. Again, the results in the decision map show consistency with the automated classifications of tissue type made by application of methods of the invention.

h. Example 8: Absorption Spectra of Prostatic Tissue

[0132] Absorption spectra analyses were performed on both healthy and malignant prostatic tissues using a Perkin Elmer absorption spectrometer at the National Institute of Standards and Technology in Boulder, Colo. The healthy tissues were obtained from a twenty-year-old donor who had no previous history of prostatic diseases. The carcinoma tissue samples were obtained from a radical retropubic prostatectomy (RRP) specimen immediately after the surgery. The frozen samples were placed on slides and OCT sealant was applied. No staining was used. A trained pathologist identified the cancer areas of the tissues samples. The results, illustrated in the graph of FIG. **26**, reveal a number of spectral features that are common to spectra of both healthy and malignant prostatic tissues as well as unique features. The amplitudes of the features vary systematically, with an intensity reversal occurring around 1400 nm. However, these spectral features lie in the region where absorption due to water is very high and hence are unsuitable for in vivo diagnostics.

i. Example 9: Fluorescence Spectra of Prostatic Tissue

[0133] As there is no published data regarding fluorescence spectra of prostatic tissue, a preliminary measurement using formalin-fixed, paraffin-embedded prostate tissue was undertaken. Using a pen, a pathologist marked prostate cancer and normal areas on a collection of haematoxylin and eosin (H&E) stained whole-mount slides. Optical measurements were taken from unstained 10 μm thick sections cut from each block adjacent to the H&E section. By carefully overlaying the pathologically classified areas on H&E slides with the corresponding unstained section, auto-fluorescence spectra were generated for normal and malignant prostatic tissue from two different patients, as illustrated in FIGS. **27**A and **27**B. The excitation source was a violet light emitting diode (LED) with an optical bandwidth of 360-410 nm and 25 μW power. Both types of tissue appear to display collagen and nicotinamide adenine dinucleotide (NADH) peaks approximately located at wavelengths of 440 nm and 490 nm, respectively.) However, fluorescence intensity levels of these fluorophores obtained from formalin-fixed tissue are much lower compared to those from fresh in vivo or ex vivo tissue samples. Therefore, the fluorescence intensities measured from formalin-fixed tissue are not useful references in clinical settings.

j. Example 10: Fluorescence Spectral of Prostate Cell Cultures

[0134] To identify specific endogenous fluorophores and their excitation and emission spectra useful in clinical settings to diagnose prostatic carcinoma in vivo, experiments may be performed using a collection of prostate cancer cell lines. An appropriate collection should be comprehensive and include prostate cell cultures that represent benign cells, cancer, and metastatic disease. The collection should constitute a variety of different types and stages of prostate cancer, while also reflecting the heterogeneous nature of this malignancy. Exemplary prostate carcinoma cell lines may include LNCaP, DU 145, NCI-H660, PC-3, ALVA-31, 22Rv1, CWR-R1, DuCaP, LAPC-4, MDA PCa 1, MDA PCa 2a, MDA PCa 2b, PC-346C, PSK-1, and VCaP, as well as BPH-1 and PrEC primary cultures of normal prostate to generate fluorescence spectra. Rhodamine-B spectra may be used to normalize between different experiments.

[0135] Cell suspensions may be prepared and placed in a quartz cuvette with 1 cm path length. A conventional laboratory fluorometer (e.g., Fluorolog-3, JY Horiba Inc., Edison, N.J.) may be used to characterize the fluorescence properties of each cell suspension. An exemplary fluorometer instrument may consist of a 450 W xenon arc lamp, double excitation and emission scanning monochromators, a sample compartment with a cuvette holder and magnetic stirrer, and a photomultiplier tube (PMT). Adjustable parameters of the instrument may include the excitation and emission wavelength ranges and increment, the excitation and emission band-passes, the high voltage of the PMT, the integration time, the stirring speed of the magnetic stirrer, and the collection geometry.

[0136] Fluorescence excitation-emission matrices may be recorded by measuring the fluorescence-emission spectra over a range of excitation wavelengths. A fluorescence EEM involves measurement of the fluorescence intensity as a function of both excitation and emission wavelengths. The excitation wavelength may be varied from about 260 to 540 nm. At each excitation wavelength, fluorescence emission spectra may be recorded from a wavelength slightly above the excitation wavelength to 700 nm. These wavelength ranges will enable characterization of all endogenous fluorophores, porphyrins, ceroid, tryptophan, NAD(P)H and FAD, likely to be present in prostate cells in the ultraviolet (UV) through visible (VIS) spectrum.

[0137] FIG. **28** and FIG. **29** illustrate EEM matrix data obtained for a DU145 cell suspension (3 million cells/ml) using Fluorolog-3. The excitation-emission frequencies of NADH and Tryptophan are known and the amounts present in benign tissue are relatively higher than in malignant tissue. The fluorescence signal is proportional to the concentrations of each fluorophore. For a DU145 cell suspension, the peak fluorescence intensity due to tryptophan (0.02 a.u.) is two-fold higher than for NADH (0.01 a.u.).

[0138] The peak fluorescence intensity for each fluorophor is determined by absorption/absorbers of the medium. For example, fluorescence from tryptophan for three different cell concentrations at wavelengths of 280 and 300 nm excitations is indicated, respectively, in FIGS. **30**A and **30**B. FIGS. **31**A and **31**B indicate fluorescence from NADH for three different cell concentrations at wavelengths of 340 and 360 nm, respectively. The peak fluorescence intensity of tryptophan for the highest cell concentration (6 million cells) is lower at 280 nm than the two lower concentrations (1.5 and 0.75 million cells). The order is reestablished, however, at 300 nm excitation. This is likely caused by an absorption feature at 280 nm and hence the absorption and scattering coefficients of the medium need to be measured to extract the "intrinsic" fluorescence spectrum.

[0139] In addition if there are non-fluorescing absorbers, then those will reduce the excitation energy at the focal volume and reduce the amount of fluorescence that reaches the detector. The larger the concentration of absorbers, the greater the reduction of excitation energy. This is called "trapping." Consequently, scattering and absorption coefficients of cell cultures need to be evaluated to recover the fluorescence signal. This is also true for tissue. Absorption is even more pronounced in biological tissue due to oxy- and deoxy-hemoglobin. An integrating sphere and a cuvette may be used to measure absorption and scattering coefficients of biological tissue and cell suspensions.

[0140] A statistical analysis was performed to determine whether fluorescence spectrum due to tryptophan is significantly different between normal (BPH-1) and malignant (DU145, PC3, DuCap, VCap) cell suspensions. For each fluorescence spectrum, data points between 3 dB cutoff points were included in the analysis. There was a statistically significant difference in the fluorescence signal due to tryptophan between normal and malignant cell suspensions at 280 and 300 nm excitations (t-test $p<0.0001$). The same was true for NADH at 340 nm excitation (t-test $p<0.0001$). It may be concluded that there is significantly more tryptophan and NADH in normal cells than in malignant cells and these differences may be utilized for tissue classification.

k. Example 11: Diagnosis of Prostatic Pathology Using Optical Probe

[0141] An optical probe was used to measure and characterize the prostatic tissue. Using data reductions, normalization, and applying artificial neural networks, identification of malignant prostatic tissue from normal prostatic tissue is demonstrable.

[0142] An exemplary invasive optical probe **1400** as shown in FIG. **14** captures ESS of prostatic tissues from ex vivo RRP specimens in the range of 200-1150 nm. Over 900 spectra of prostatic tissues from 52 RRP patients were collected using a 22 gauge optical probe (custom-made by Ocean Optics, Dunedin, Fla.). The optical probe **1100** may be inserted into an 18-gauge biopsy needle to provide in vivo access to the prostate. A tungsten/halogen light source provides illumination over the wavelength range 360-2000 nm. The light source is coupled to a 200 μm optical fiber selected to transmit over the wavelength range of interest. The probe consists of a bundle of 14 optical fibers. There are six UV-VIS (200-750) and six VIS-NIR (450-1100) illumination fibers arrayed around two read fibers, one UV-VIS and one VIS-NIR. The two read fibers are coupled to an Ocean Optics 52000 double spectrometer with CCD detectors. A laptop computer is used to control the system and collect data.

[0143] Tissue spectra collected from each location were recorded with a unique identifier providing precise information of the location. After collecting tissue spectra from the near-end of the optical probe, a corresponding biopsy was taken from each location. Each sample was polarized using blue ink to identify the near-end of the biopsy core. The biopsy samples were spot-frozen in OCT compound using a dry ice/isopentane bath for standard pathological classification. After the data collection, RRP specimens were fixed in 10% neutral-buffered formalin (NBF) to generate whole-mount sections.

[0144] A trained pathologist may use standard pathological methods to review routine 5 μm H&E stained biopsy specimens. Each of the slides may be evaluated for the presence of carcinoma, denoted by Gleason sum (primary Gleason grade+secondary Gleason grade), prostatic intraepithelial neoplasia (PIN), acute prostatitis, chronic prostatitis, cystic atrophy, simple atrophy, basal cell hyperplasia, atypical adenomatous hyperplasia, and various subtypes of benign prostatic hyperplasia (BPH) nodules (adenomatous, fibroadenomatous, fibromyoadenomatous, fibromatous, and leiomyomatous). This data may be recorded identifying every mm length as well as a gross classification of the near-end (inked-end), middle, and far-end of the biopsy sample. In addition, each biopsy sample may be scored as Good, Adequate, or Inadequate with respect to biopsy quality. Biopsy classification data may be collected and entered into a relational database to be later correlated with the spectra taken for each sample.

[0145] The advantage of having spectral data in the relational database is that it provides the capability to reduce and normalize these data in a variety of ways. In an exemplary data reduction and normalization scheme for newly acquired spectral data, the lowest amplitude observed in the entire population may be subtracted from each data point. Normalized amplitude values may be obtained by dividing the amplitudes by the mean amplitude calculated across each specific case. The final data set may be composed of mean amplitudes over a preset wavelength range, thus condensing the data points into a more manageable representation.

[0146] Initial screening of tissue biopsy classification based on biomorphometric data from whole-mount sections and three-dimensional computer models should be able to pick most outliers and line-sitters. Other techniques such as logistic regression and linear discriminant analysis may also be used. Further, non-linear approaches such as ANN, Gaussian processes, and support vector machine algorithms may be employed.

[0147] Determining the best choice of diagnostic test parameters is important. The prostatic tissue classification scheme must be able to predict a minimum of two possible outcomes (benign versus malignant) and more than two if Gleason sum classification of malignant tissue and PIN are

to be included. A simplified classification scheme incorporating Gleason sum and PIN requires 16 possible outcomes whereas a comprehensive classification requires 26 possible outcomes. Determining 16 test parameters may be realized, for example, by dividing a 300-900 nm spectrum into 20 nm bands, which results in about 30 bands, each band providing one test parameter. Absorption features and slope variations that discriminate benign versus malignant tissue may also be used. Other possible parameters may include peak height ratios and factor analysis based on dividing the spectrum into domains. Factor or cluster analysis methods may also be helpful to identify promising groupings of the available data.

[0148] The diagnostic thresholds are sets of values of the diagnostic test parameters that determine the diagnostic outcome, i.e., no cancer, cancer or cancer grade, and the various benign conditions. A set of values for diagnostic thresholds may be determined based on their ability to properly predict the outcome, which may be assessed using standard medical measures. These measures include sensitivity, specificity, positive predictive value, negative predictive value, and test efficiency.

[0149] A preliminary ANN trained on spectral data from the UV-visible read fiber has been able to classify benign versus malignant tissue at 65-70% sensitivity. To eliminate outliers and improve the correlation of spectral data with pathological classification, pathological information from whole-mount sections was used to reconstruct three-dimensional computer models of RRP specimens. Pathological classification and tissue spectra were not the same due to several problems with this setup. First, some spectra may have been captured 5-10 mm away from the location where the biopsy was taken due to operator error. Second, the intensity of light sources and wide field of view of the probe may have excited surrounding tissue where spectral data for each biopsy could no longer be localized to the near end. An ANN trained on a reduced data set by eliminating the suspected outliers achieved a near perfect classification (sensitivity and specificity >90%) of normal versus malignant tissue (e.g., as shown in FIGS. **7**A and **7**B).

[0150] Having described several embodiments, it will be recognized by those of skill in the art that various modifications, alternative constructions, and equivalents may be used without departing from the spirit of the invention. Accordingly, the above description should not be taken as limiting the scope of the invention, which is defined in the following claims.

1.-**29**. (canceled)

30. A system for real-time classifying an in vivo location of prostate tissue within a prostate of a patient, the system comprising:

an optical probe comprising a needle having a tip, wherein at least a portion of the needle is configured to penetrate the prostate so that the tip is directed toward the in vivo location of prostate tissue, and wherein the optical probe is configured to transmit light to the in vivo location and obtain received light from the in vivo location;

a spectrometer connected with the optical probe, wherein the spectrometer generates optical spectral data from the received light; and

a computational device comprising

at least one component which translates the optical spectral data into digital data, and

a relational database, wherein the relational database comprises a plurality of correlations between known digital data and classifications wherein each of the plurality of correlations were generated by

a) in vivo capture of received light from a test location within a prostate of a test patient,

b) generation of test optical spectral data from the received light from the test location,

c) generation of the known digital data from the test optical spectral data,

d) histological evaluation of an excision of the test location to determine a classification corresponding to the known digital data,

wherein the computational device compares the digital data to the known digital data of the relational database and provides a real time classification based on at least one of the plurality of correlations.

31. A system as in claim **30**, wherein the classification comprises benign, malignant, abnormal, cancerous, dysplastic, diseased or calcified.

32. A system as in claim **30**, wherein the classification comprises high grade disease or low grade disease.

33. A system as in claim **30**, wherein the optical spectral data comprises fluorescence from at least one endogenous fluorophore within the in vivo location.

34. A system as in claim **33**, wherein the at least one endogenous fluorophore comprises tryptophan, tyrosine, phenylalanine, collagen, elastin, FAD, flavins, NADH, NADPH, Vitamin A, Vitamin K, Vitamin D, pyridoxine, pyridoxamone, pyridoxal, pyridoxic acid, pyridoxal 5'-phosphate, Vitamin B12, phospholipids, lipofuscin, ceroid, and/or porphyrins.

35. A system as in claim **33**, wherein the optical spectral data comprises elastic scattering spectra reflected from the in vivo location.

36. A system as in claim **30**, wherein the optical probe includes at least one transmitting fiber extending to the tip so as to transmit the light from at least one light source to the in vivo location and to transmit the received light from the in vivo location.

37. A system as in claim **36**, wherein the at least one transmitting fiber has a distal end which is flush with a blade surface of the tip of the optical probe.

38. A system as in claim **36**, wherein the tip of the optical probe has an aperture configured to restrict the light from the at least one transmitting fiber so that the in vivo location has a size of a point.

39. A system as in claim **30**, wherein the optical probe includes at least one transmitting fiber extending to the tip so as to transmit the light from at least one light source to the in vivo location and at least one optical fiber extending from the tip so as to transmit the received light from the in vivo location.

40. A system as in claim **30**, wherein the needle of the optical probe is advanceable so as to direct the tip toward a new in vivo location of prostate tissue without removing and reintroducing the optical probe to the prostate, and wherein the computational device provides a new real time classification for the new in vivo location.

41. A system as in claim **30**, wherein the optical probe includes a mechanism for delivering a therapeutic agent to the in vivo location.

42. A system as in claim **30**, wherein the optical probe includes a mechanism for delivering a therapeutic modality to the in vivo location.

43. A system as in claim **42**, wherein the therapeutic modality comprises brachytherapy or cryotherapy.

44. A system as in claim **30**, wherein the at least one component generates an excitation emission matrix (EEM) based the optical spectral data, wherein the EEM derives a plurality of spectral measures are used in translating the optical spectral data into digital data.

45. A system as in claim **30**, wherein the at least one component comprises an artificial neural network that searches for differentiating features of the optical spectral data, wherein the differentiating features are used in translating the optical spectral data into digital data.

46. A system as in claim **30**, wherein the at least one component comprises diagnostic spectroscopy software for analyzing the optical spectral data when translating the optical spectral data into digital data.

47. A system as in claim **30**, wherein the at least one component comprises at least one support vector machine algorithm for analyzing the optical spectral data when translating the optical spectral data into digital data.

48. A system as in claim **30**, further comprising a light source which generates the light, wherein the light source comprises at least one bandwidth-limited incident light source in the UV or near UV spectrum.

* * * * *